Energy 260 (2022) 125191

Contents lists available at ScienceDirect

Energy

journal homepage: www.elsevier.com/locate/energy

A comprehensive CFD study of the spray combustion, soot formation and emissions of ternary mixtures of diesel, biodiesel and gasoline under compression ignition engine-relevant conditions

Mohammad Zandie [a], Hoon Kiat Ng [a,*], Suyin Gan [b], Mohd Farid Muhamad Said [c], Xinwei Cheng [d]

[a] Department of Mechanical, Materials and Manufacturing Engineering, University of Nottingham Malaysia, Jalan Broga, 43500, Semenyih, Selangor Darul Ehsan, Malaysia
[b] Department of Chemical and Environmental Engineering, University of Nottingham Malaysia, Jalan Broga, 43500, Semenyih, Selangor Darul Ehsan, Malaysia
[c] Automotive Development Center (ADC), Faculty of Engineering, Universiti Teknologi Malaysia (UTM), 81310, Johor Bahru, Malaysia
[d] School of Mechanical and Aerospace Engineering, Queen's University Belfast, Northern Ireland, UK

ARTICLE INFO

Keywords:
Diesel/biodiesel/gasoline
Spray/flame development
Spray combustion
Soot formation
Computational fluid dynamics
Emission gases

ABSTRACT

In this research, the spray combustion, soot formation and exhaust emissions of diesel, biodiesel, gasoline fuels and their mixtures are analysed in a constant volume chamber. A multicomponent kinetic mechanism (CDBG) suitable for diesel-biodiesel-gasoline mixtures developed by our research group is utilised, and the associated physicochemical properties are thoroughly calculated. Adaptive mesh refinement scheme with appropriate mesh independency analysis are applied. Liquid penetration length, lift-off length, ignition delay and soot formation have been benchmarked against experimental data in the literature. A hybrid RANS-LES model, known as DES model, is used to simulate the turbulent condition. The effects of different ambient temperature/oxygen levels on the flame structure, soot formation and emissions of different ternary mixtures of D75|BD20|G5, D70|BD20|G10 and D65|BD20|G15 were analysed. D65|BD20|G15 resulted in a lower soot mass yield than that of BD100 (pure biodiesel) and D100 (pure diesel) for about 35% and 27%, respectively, at T = 900 K | O_2 = 15%. Greater soot mass reductions for the tested fuels were captured by the decrease in ambient temperature from 900 K to 800 K by a factor of ~1/3 (same ambient O_2 concentration). Lower nitrogen oxides (NO_x) emissions were obtained for D100 by factors of ~1/2 at T = 900 K | O_2 = 15% compared to BD100. Gasoline-added mixtures revealed lower NO_x compared to BD100 (~20%) yet still higher than D100. Lower carbon dioxide (CO_2) and carbon monoxide (CO) emissions were captured for D65|BD20|G15 compared to BD100 and D100.

1. Introduction

1.1. Emerging novel fuelling technologies and associated challenges

The exacerbated exploitations of petroleum-based fuels in a myriad of industries, particularly the transportation sectors, have brought about international concerns such as fossil fuels depletion, hastened climate change and more importantly jeopardised human well-being [1,2]. These hazards have inclined researchers and involved industries to seek alternative energy resources to address the concerns associated with conventional fuelling strategies and reduce global reliance on petroleum-based fuels as primary energy source. In addition, this alternative energy resource must also be economically viable, renewable, practically manageable for large-sized adaptations, and more importantly, meet the fuel economy and power demands of the end-users. Of the most applicable proposed alternative fuels in recent decades is biodiesel. The reason behind its popularity could be assigned to its biodegradability, abundance, non-toxicity and compatibility with current industrial infrastructures and different engine setups [3]. Various studies have sought to analyse the emission give-outs of diesel-biodiesel mixtures and the results authenticated the hypotheses made. As such, considerable reduction in carbon dioxide (CO_2), particulate matter (PM), sulphur dioxide (SO_2) and unburnt hydrocarbons (UHCs) was achieved by integrating biodiesel. However, the results associated with nitrogen oxides (NO_x) are deemed inconclusive. Despite

* Corresponding author.
E-mail address: hoonkiat.ng@nottingham.edu.my (H.K. Ng).

https://doi.org/10.1016/j.energy.2022.125191
Received 10 May 2022; Received in revised form 11 July 2022; Accepted 15 August 2022
Available online 19 August 2022

Nomenclature

A4	Pyrene
AMR	Adaptive mesh refinement
B0	Model constant
B1	Model constant
BD100	Pure biodiesel
C_2H_2	Acetylene
C_3H_3	Propargyl
C_4H_4	Cyclobutadiene
C_6H_{12}	Cyclohexane
$C_{13}H_{26}O_2$	Methyl laurate
$C_{15}H_{30}O_2$	Methyl myristate
$C_{17}H_{34}O_2$	Methyl palmitate
$C_{19}H_{38}O_2$	Methyl stearate
$C_{19}H_{36}O_2$	Methyl oleate
$C_{19}H_{34}O_2$	Methyl linoleate
$C_{19}H_{32}O_2$	Methyl linolenate
$C_{21}H_{44}$	Heneicosane
CDBG	Compact combined diesel-biodiesel-gasoline kinetic mechanism
CFD	Computational fluid dynamics
CI	Compression ignition
CL	Break-up length constant
CO	Carbon monoxide
CO_2	Carbon dioxide
CRT	Model constant
Ctau	Model constant
D65|BD20|G15	65% Diesel +20% Biodiesel +15% Gasoline
D70|BD20|G10	70% Diesel +20% Biodiesel +10% Gasoline
D75|BD20|G5	75% Diesel +20% Biodiesel +5% Gasoline
D100	Pure diesel
DES	Detached Eddy Simulations
DRG	Directed Relation Graphs
DRGEP	Directed Relation Graph with Error Propagation
FAME	Fatty acid methyl ester
G50BD50	50% Gasoline +50% Biodiesel
G70BD30	70% Gasoline +30% Biodiesel
GCI	Gasoline compression ignition
HFDBIE	High-frequency diffused background illumination extinction
HPC	High performance computing
ID	Ignition delay
KH-RT	Kelvin–Helmholtz–Rayleigh–Taylor
LES	Large Eddy Simulation
LOL	Lift of length
MB	Methyl butanoate
MD	Methyl decanoate
N_2O	Nitrous oxide
N_2O_3	Dinitrogen trioxide
N_2O_5	Dinitrogen pentoxide
NO	Nitric oxide
NO_2	Nitrogen dioxide
NO_x	Nitrogen oxides
O_2	Oxygen
OH	Hydroxide
PAH	Polycyclic Aromatic Hydrocarbon
PME	Palm methyl ester
RANS	Reynolds Averaged Navier Stokes
T	Temperature
TCI	Turbulence-chemistry integration
URF	Under relaxation factors
WCO	Waste cooking oil biodiesel
2-D	2-Dimensional
3-D	3-Dimensional

the beneficial aspects of using biodiesel, a trade-off between the positive emission suppression features and lower heating values for this fuel was reported [4]. This downside could adversely deteriorate the engine power output.

Therefore, pure biodiesels are not quite utilisable in the current diesel/compression ignition (CI) engines unless appropriate modifications are incorporated. This is mainly due to the low ignitability and poor spray liquid characteristics of biodiesel compared to diesel [1,5]. Several techniques have been examined in recent decades including fuel additives (nano-particles), pre-chamber fuel preheating, etc., however, they are not deemed practically implementable on a large-scale. Recently, the mixing of biodiesels with conventional fuels such as diesel or gasoline has been deemed a popular solution to this matter. As such, it has been discerned that utilising biodiesel-diesel blends in existing diesel/CI engines even without any modifications could commendably improve the overall combustion performance and inhibits engine-out emissions [6,7]. On the other hand, numerous investigations have scrutinised the integration of biodiesel-gasoline blends to relieve the impediments associated with diesel/CI engines functionalities. The mixing of gasoline comes with significant benefits including, improved atomisation process, enhanced fuel properties, prolonged ignition delay (ID) timing and hence, promoted air-fuel mixing process and diminished soot formation [8]. As a result of the above benefits for gasoline integration, further NO_x and PM suppression were achieved when multiple injection and exhaust gas recirculation techniques were applied.

1.2. Advances in spray combustion modelling of dual and ternary fuelling strategies using CFD

Recently, Xu et al. [9] studied the formation of nitrogen oxides and soot formation in n-heptane/methanol dual-fuel combustion using Large Eddy Simulation (LES). In their investigation, the impacts of methanol on pollutants productions under different ambient temperatures were analysed. It was ascertained that the soot formation in dual-fuel combustions follows a non-linear dependency on the change in ambient temperature; as such, soot emission was suppressed at low temperatures, while it is enhanced at high temperatures. Also, an improved mixing process was found as the main factor for soot reduction in low to moderate temperatures, whereas, shortened lift-off length (LOL) and lower ambient oxygen content were deemed accountable for higher temperature cases. Zhong et al. [10] conducted an analysis on the ignition process, lift-off evolution and emission gases of n-heptane/syngas dual fuelling combustion using LES model. The flame structure in their case was found to be noticeably changing, due to the different regimes of flame structure and auto-ignition phenomena in dual-fuelling scenarios. Zhang et al. [11] investigated the spray development, flame combustion and emission characteristics of diesel engine fuelled with diesel/methanol/n-butanol mixtures using a 3-D CFD model. In their research, an optimum blending scenario for the respective mixture was proposed, under which the emission gases were significantly diminished. The overall performance and combustion process of the engine was also found to be enhanced for the integrated ternary fuelling mixture compared to the pure diesel case. In another study, Kuti et al. [12] simulated the spray combustion characteristics of waste cooking oil biodiesel (WCO) and diesel fuels using a Reynolds Averaged Navier

Stokes (RANS) k-ϵ turbulent model. The effects of fuels blend formation on combustion as well as the stabilizing mechanism of lifted flame were also meticulously studied. Zhong et al. [8] attempted to perform a CFD analysis on the spray/flame development and soot emission of biodiesel-gasoline mixture in a constant volume chamber. In their investigation, a reduced kinetic mechanism was developed that was equipped with a reduced Polycyclic Aromatic Hydrocarbon (PAH) mechanism. Their proposed mechanism along with the phenomenological soot model showed acceptable results in capturing the spray characteristics and soot formation of the respective mixture under gasoline compression ignition-like conditions (GCI). In addition, the effects of ambient temperature and oxygen level on flame development and soot production were extensively analysed. In another investigation, Pischke et al. [13] analysed the influence of different turbulence models for emulating the turbulence structures of a hollow-cone spray. In their study, the results obtained through using detached eddy simulation (DES) was compared with LES and RANS models, and it was found that the DES model can acceptably handle free jet turbulence quite similar to the LES model. Moreover, it was also outlined that DES model combines the beneficial aspects of LES and RANS simulation in predicting the turbulent behaviour of the spray. Sehole et al. [14] also simulated turbulent spray combustion in a turbo jet combustor to predict the NO_x concentration using DES model. The model could acceptably capture the temperature distributions within the chamber compared to the experimental data. Their findings indicated that the DES model is a potential scheme for predicting multiphase reactions in real-world gas-turbine combustion chambers.

1.3. Novelty and objectives of this study

Given the proliferation achieved in the high-performance computing (HPC) powers, there is a noticeable inclination in both industrial and academic research toward analysing the spray combustion and emission characteristics of novel fuelling strategies using more accurate modelling approaches. The turbulent model as an example is deemed as a critical choice in modelling dual/ternary fuel mixture combustions. The k-ϵ model was being extensively employed over the past decades, however, recently better resemblance with respect to the experimental findings has been achieved for LES turbulent model due to its high fidelity in replicating turbulence-related phenomena [15]. It is to be noted that LES model comes with a high computing power requirement and is mostly used for 3-D simulations, whereas, Detached Eddy Simulations (DES) model, as a hybrid RANS/LES model, has gained much attention in 2-D combustion simulations [16–18]. The DES turbulent model can viably switch to Large Eddy Simulation (LES) model in detached regions and therefore, cutting the computational cost/time noticeably and yet still offering most of LES methods advantages [19]. Therefore, in this study the spray/flame structure of diesel/biodiesel/gasoline mixtures have been simulated using DES turbulent model.

Moreover, CFD is found as a robust and useful tool in grasping a better understanding of the combusting behaviour as well as emission characteristics in dual/ternary fuelling mixtures [20]. Such numerical analyses could feasibly unearth the real-life combustion phenomena via meticulously scrutinising reactants, spray/flame development and engine-out products [21]. Nevertheless, the direct combustion modelling of practical fuels is sought to be impractical since they generally comprise of a large number of components with high complexities. Therefore, fuel surrogates with simplified molecular structures can viably emulate the combustion characteristics of the intended fuels with great accuracy and manageable computational requirements.

Furthermore, so far there has been only a limited number of experimental/numerical investigations concerning the combustion characteristics of diesel/biodiesel/gasoline mixtures [22,23]. Henceforth, the objective of the current research is to broaden the understanding of the previously obtained experimental observations using CFD simulation. To this end, the spray/flame development and soot formation of diesel/biodiesel/gasoline fuels and their mixtures have been simulated in a 2-D constant volume chamber under compression ignition (CI) engine-like conditions. A novel reduced multicomponent kinetic mechanism for diesel-biodiesel-gasoline mixtures (CDBG mechanism) with 369 species/1647 reactions developed by our research group has been incorporated in this study [2]; in which, in order to accurately characterise the ignition characteristics of diesel/biodiesel/gasoline fuels and their mixtures, an accurate set of kinetic mechanisms were integrated encompassing n-heptane as diesel surrogate, methyl-butanoate (MB) and methyl-decanoate (MD) as biodiesel surrogate and iso-octane and toluene as gasoline surrogates. The developed reduced CDBG mechanism was capable of emulating the combustion characteristics of the abovementioned fuels with different aspects such as C/H ratios under a diverse range of operating conditions. This mechanism is then employed here to meticulously scrutinise the phenomena involved in spray/flame development, soot production and exhaust emissions of the fuel mixtures, for which experimental studies may be unable to provide detailed justifications.

The evaluation of physicochemical properties for the integrated fuels is another critical stage in accurately studying the combustion-related processes. Thus, in this study it is attempted to calculate a comprehensive array of physicochemical properties comprised of 15 liquid, vapour and critical properties under a wide range of operating conditions while importing into the CFD solver's library. This study can be deemed as a pioneering work in evaluating the spray combustion and soot formation of ternary fuelling strategy for diesel-biodiesel-gasoline fuels using CFD simulations that utilises a reduced compact combined multicomponent mechanism equipped with a practical phenomenological soot model. Also, the influences of different parameters on the spray/flame development, soot formation, exhaust emissions as well as important precursor species were examined. The results achieved for liquid penetration length, flame lift-off length, ignition delay timing and soot formation were in great agreement with experimental data. The outcomes of this CFD analysis are expected to provide insightful analysis into the spray/flame development, fuel mixture, soot pollutant and emission gases of diesel-biodiesel-gasoline that come in handy in CI engines.

2. Experimental data

The experimental data utilised to validate the simulation results are retrieved from the works of Zhong et al.'s research group [24–26] consisting of liquid penetration length, flame lift-off length, ignition delay and soot production in a spray flame. Throughout the experiments the fuels were injected into a constant volume cylindrical chamber with a volume of 12 L. Specific details about the chamber design, measurement methods and high-frequency diffused background illumination extinction (HFDBIE) approach are provided in the literature [7,24,27]. A single-hole injector system with an orifice diameter of 0.12 mm and injection pressure of 80 MPa was utilised to inject the fuel into the chamber. Pure biodiesel, pure diesel and gasoline-biodiesel mixture by volume ratios of 50%/50% and 70%/30% (G50BD50 & G70BD30) were employed as the target benchmarks in this study. It is to be mentioned that in this study an accurate multicomponent kinetic mechanism that has been recently developed by our research group is employed, which is suitable to capture the combustion characteristics of diesel, biodiesel, gasoline fuels and their mixtures. Also, a comprehensive set of associated physicochemical properties is also calculated, which entails 15 important features. These two important aspects, which have also been urged in previous studies [8], are hypothesised to increase the reliability and accuracy of the simulation outcomes compared to experimental data.

3. Physicochemical properties development

The estimation of physicochemical properties is of paramount

importance since it has been ascertained that important phenomena such as mixing phase, spray development and overall combustion performance are greatly dependent on the variation in physicochemical properties [28,29]. To this end, the physicochemical properties of diesel, biodiesel and gasoline have been meticulously calculated, which comprise 15 properties for vapour, liquid and critical properties. As shown in Fig. 1, these properties are plotted against a temperature range of 280 K up to the respective critical temperature of each fuel. As for the biodiesel physicochemical properties, the physicochemical properties of palm methyl ester (PME) have been used and the properties were evaluated according to the actual fuel compositions given in Table 1.

The methods of evaluation in this study to calculate the physicochemical properties are presented in Table 2. A point to be highlighted here is that throughout the vapour diffusivity evaluation, an enhancement is made to integrate the air/fuel binary interaction, which is proposed by the Lennard-Jones potential [30] whereas in other research, binary interactions between the FAME components were taken into consideration [28].

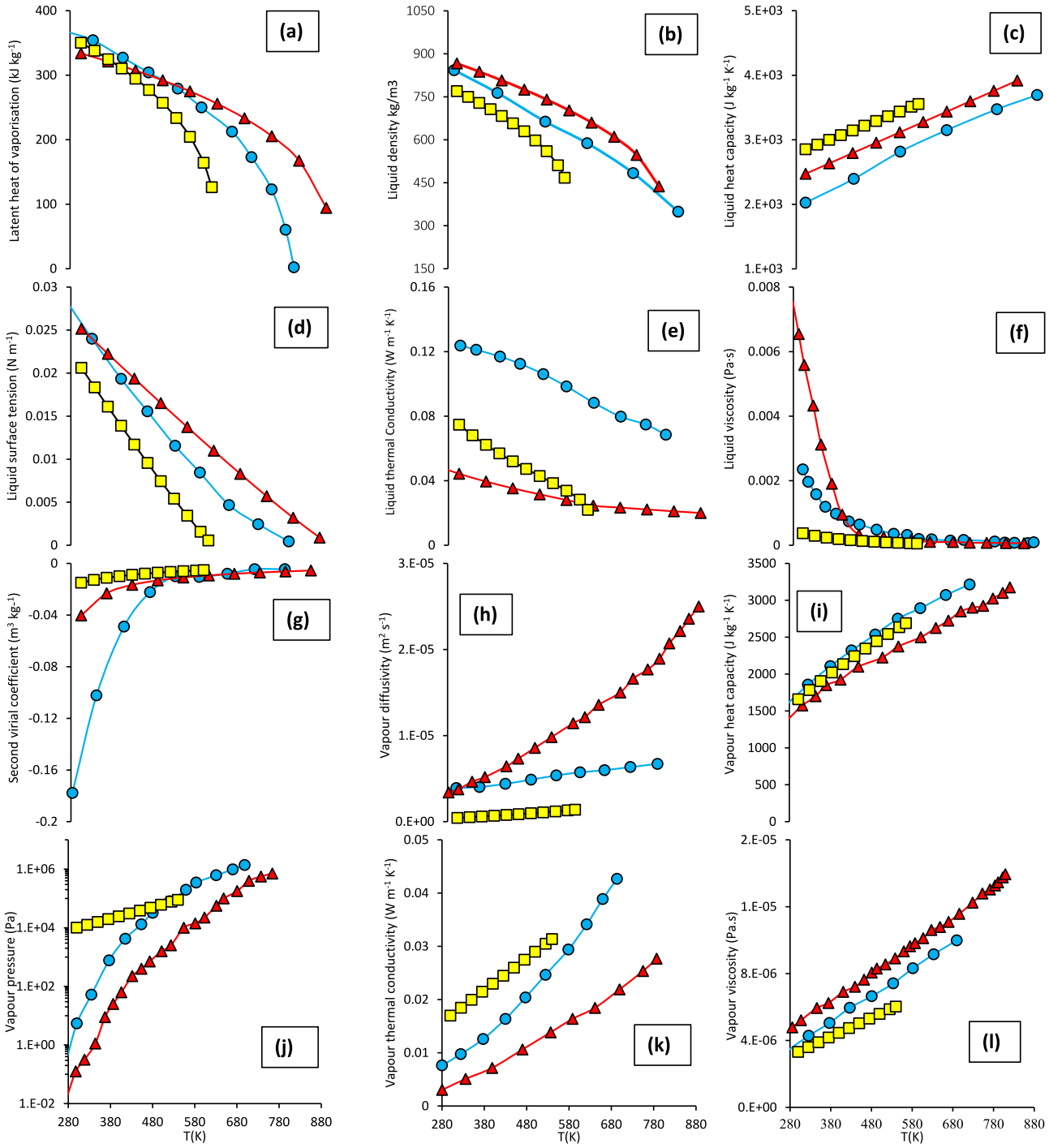

Fig. 1. The physicochemical properties of diesel (blue line-sphere markers), biodiesel (red line-triangle markers) and gasoline (black line-square markers) over temperatures of 280 K up to the respective critical temperatures of each fuel for (a): heat of vaporisation, (b): liquid density, (c): liquid heat capacity, (d): surface tension, (e): liquid thermal conductivity, (f): liquid viscosity, (g): second-virial coefficient, (h): vapour diffusivity, (i): vapour heat capacity, (j): vapour pressure, (k): vapour thermal conductivity and (l): vapour viscosity.

Table 1
The PME composition according to the saturation and unsaturation levels [28,29].

FAME[b] component	Fuel
	PME (%)[a]
Saturated	
Methyl laurate ($C_{13}H_{26}O_2$)	–
Methyl myristate ($C_{15}H_{30}O_2$)	1.0
Methyl palmitate ($C_{17}H_{34}O_2$)	42.0
Methyl stearate ($C_{19}H_{38}O_2$)	5.0
Unsaturated	
Methyl oleate ($C_{19}H_{36}O_2$)	41.0
Methyl linoleate ($C_{19}H_{34}O_2$)	10.0
Methyl linolenate ($C_{19}H_{32}O_2$)	–
Saturation level (%)	Nearly 50.0
Unsaturation level (%)	Nearly 50.0

[a] Based on Ismail et al. [28].
[b] Short for fatty acid methyl esters.

Table 2
Methodologies used to evaluate the thermophysical properties.

Properties	Evaluation methodology	References
Boiling point	Experiment	
Critical temperature	Joback modification of Lydersen's method	[30]
Critical volume	Joback modification of Lydersen's method	[30]
Critical pressure	Joback modification of Lydersen's method	[30]
Latent heat of vaporisation	Pitzer acentric factor correlation	[36]
Liquid density	Modified Rackett equation	[30]
Liquid heat capacity	Van Bommel correlation	[37]
Liquid surface tension	Correlation proposed by Allen et al.	[38]
Liquid thermal conductivity	Robbin and Kingsrea method	[30]
Liquid viscosity	Orrick and Erbar method, Letsou and Stiel method	[30]
Second virial coefficient	Tsonopoulos method	[30]
Vapour diffusivity	Lennard-Jones potential, Wilke and Lee method	[30,36]
Vapour heat capacity	Rihani and Doraiswamy method	[30]
Vapour pressure	Modified Antoine equation	[39]
Vapour thermal conductivity	Correlation by Chung et al.	[40,41]
Vapour viscosity	Correlation by Chung et al.	[40,41]

On the other hand, as for the diesel fuel, n-tetradecane is chosen to represent the diesel fuel's physicochemical proprieties, which is comprised of fuel ranges from cyclohexane (C_6H_{12}) to heneicosane ($C_{21}H_{44}$) as determined by Lin and Tavlarides [31]. Since its physicochemical properties were ascertained to be 92% analogous to those of practical diesel fuel. Therefore, the associated properties have been then retrieved from the fuel properties library of OpenFOAM and have been integrated in this study. However, it must be noted that Lin and Tavlarides [31] also examined further incorporation of the diesel fuel surrogate components, which was proven to be in closer agreement with experimental data. Thus, in case of the liquid density, liquid heat capacity, liquid viscosity and liquid thermal conductivity the data reported by Lin and Tavlarides [31] have been adopted which integrates more diesel fuel components.

Moreover, the physicochemical properties of toluene, iso octane and n-heptane have been taken up to represent the gasoline fuel [32,33]. It must be pointed out that it is imperative to carefully define the compositions for the components chosen here for gasoline since the blending ratio can greatly affect the evaporation process, ignition delay, reactivity, etc. Henceforth, bearing in mind that extensive experimental data are used in this study to validate the later outcomes, the proportions were varied in such a way that the experimentally reported data could be regenerated. To be precise, given the distinct properties of the abovementioned components, varying the blending ratio forms arbitrary gasoline fuels with dissimilar physicochemical properties. By a series of trial and error, the optimum blending ratio was found to be 61% iso-octane, 7% n-heptane and 32% toluene. Under this circumstance, the properties reported in the reference papers [24–26] were accurately estimated with marginal errors, for the particular given temperature. It is worthy to highlight that the trial and error was according to the individual properties for each of the above components.

Afterwards, appropriate mixing rules have been integrated to evaluate the associated properties for the temperature range of interest. In addition, the estimated physicochemical properties of biodiesel and gasoline are benchmarked against those of calculated for diesel [29]. This approach is in accordance with the studies of Ra et al. [34] and Chakravarthy [35], which is due to the dearth of adequate gasoline' and biodiesel's physicochemical properties measurements under a broad range of temperatures in previous studies. The calculated physicochemical properties for the respective fuels were then imported into the fuel libraries of CFD Fluent to be used throughout the simulations. To be more exact, throughout the properties calculations, each fuel was treated individually with its own distinct physicochemical properties. Afterwards, the properties were plotted against temperature (see Fig. 1). Then, these properties were imported into the fuels properties library of Fluent, where each property was defined with Piecewise-Polynomial coefficients and the coefficients were retrieved from the line graphs in Fig. 1. The software automatically estimated the associated properties according to the blending ratios given, boundary conditions (such as temperature), initial conditions, etc using an in-built algorithm. The results obtained reveal negligible errors between the spray development with the experimental data, which suggests that this approach was reliable though for future works, the estimation of diesel-biodiesel-gasoline mixtures properties can be considered for enhanced accuracy of the simulation outcomes.

4. Numerical simulation

In this investigation, the fuel spray and the combustion of diesel, biodiesel and biodiesel-gasoline mixture have been simulated using CFD Fluent 2019-R1. The Kelvin–Helmholtz–Rayleigh–Taylor (KH-RT) model is utilised to model the spray breakup phenomenon [8,42], and the Detached Eddy Simulation turbulent model has been employed to model the turbulent condition. The dynamic-drag model is used to model the associated drag parameters. In addition, the Moss-Brookes soot model was used to model the soot formation produced by the integrated fuels. Moss-Brookes soot model allows defining the soot precursors as well as species involved in surface growth. The following sections are allocated to capture the optimum values for the abovementioned model parameters that are deemed important throughout the simulations.

4.1. Mesh independency analysis

Since a well-structured mesh design warrants more reliable modelling results, avoids computational stiffness and more importantly improves the simulation prediction competency, it is then attempted to perform a mesh independency analysis in this study prior to conducting the tests [21]. Generally, mesh structures that come with high resolutions require the least change in cell length size from one cell to adjacent cells. Therefore, assuring a smooth growth in cell size is of vital necessities in the meshing process that must be paid attention to avoid poor computational outcomes [43]. Analogous to the experimental models mentioned in Section 2 (Experimental data), a cylindrical domain with dimensions of 100 × 120 mm is designed to model the constant volume chamber. The sdaptive mesh refinement (AMR) approach is employed to mesh the structure with an initial grid size of 0.5 mm as presented in Fig. 2. Of the most beneficial aspects of using AMR meshing method is to

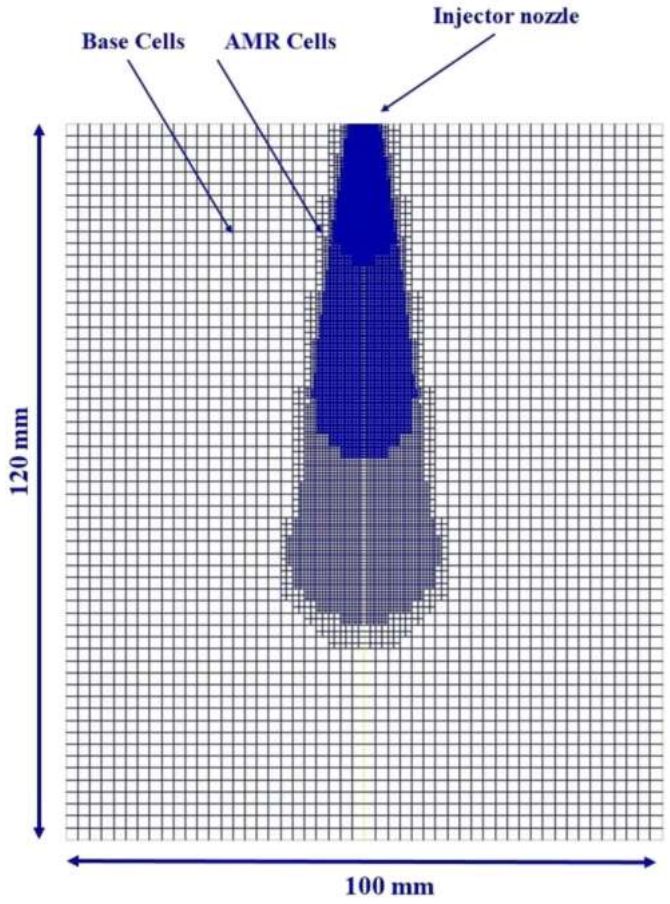

Fig. 2. Schematic of the grid structure created by AMR.

avoid using refined meshes in domains where no computational results of interest will be taken. As such, in this study those cells adjacent to the injector area/fuel spray are deemed important, therefore, the cell refinement is designed to affect this vicinity. To this end, among the available regional features that can be defined for mesh refinement, the field variable of species is chosen, whereas, cell regions with a species mass fraction more/less than a user-defined threshold are assigned to be refined.

Furthermore, three different refinement levels of 1, 3 and 5 are incorporated to meticulously discern the optimum cell sizes in the vicinity of spray devolvement, while spray penetration length of diesel (D100) is employed to validate the results predicted. It is to be noted that refinement levels will automatically refine the cells (that fall into the given criteria) to 1, 3 or 5 equally spaced cells on each side (refinement level of 1 corresponds to no refining on the current mesh). For simplicity purposes, from this point onward pure biodiesel is denoted as BD100 while G50BD50 and G70BD30 stand for gasoline/biodiesel mixtures of 50%/50% and 70%/30% by volume, respectively. Liquid penetration length is one of the useful parameters to analyse the fuel spray development. It is important to hint that the spray penetration plays a significant role since over-penetration can improve the air-fuel mixing process, yet it can also engender wall impingement [8]. Therefore, it is imperative to truly understand the liquid phase extend for the intended fuel spray. Throughout the simulations the liquid penetration length is defined as the maximum axial distance from the nozzle to the locations where the liquid fuel mass fraction of the integrated fuel reaches 97% [8, 29]. As it can be seen from Fig. 3(a), the predicted penetration length tends to diverge sharply after 0.5 ms for refinement level of 1. Meanwhile, refinement levels 3 and 5 emulate more accurate predictions of spray penetration length, however, as for 3 refinement level the results

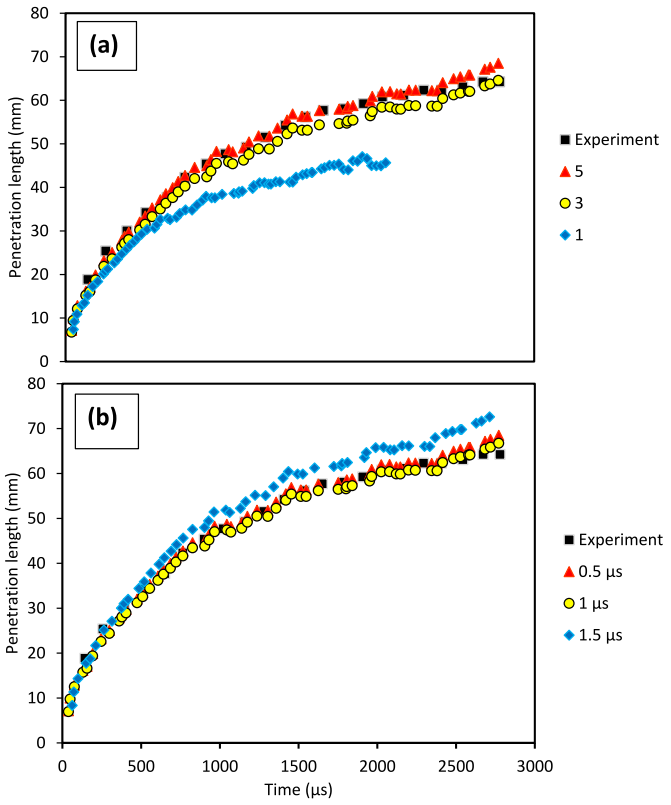

Fig. 3. Penetration length of D100 versus the (a): maximum refinement level and (b): temporal resolution and experimental data [25].

are marginally under-predicted, hence 5 refinement level is chosen. Furthermore, different AMR parameters were chosen to refine the mesh where needed. As such, since temperature and species mole fractions are of the highest interest, one AMR criteria was adopted for temperature with a gradient sensitivity of 0.3 and one for fuel species with a solution sensitivity of 0.05. Thus, cells with higher values would be refined accordingly. Additionally, given that the meshing is changing throughout the simulation, there is no fixed number of cells but the peak number of cells for the adopted conditions is found to be 72,000 and 48,000 for 5 and 3 refinement levels, respectively.

Moreover, temporal resolution is another important criterion in mesh independency analysis. For this reason, three time-steps of 0.5, 1 and 1.5 μs were tested. The results in Fig. 3(b) reveal that the penetration length for time-step of 1.5 μs is over-predicted. Whereas, time-steps of 0.5 μs and 1 μs replicate the line trend more accurately, but since the time step of 1 μs comparatively gives results as accurate as the 0.5 μs case, it is then selected as the optimum time-step.

4.2. Model parameters optimisation

The spray breakup is deemed of highly influential parameter not only for the fuel spray distribution but also in other subsequent processes including fuel consumption, air-fuel mixing, combustion and emission production [29]. Therefore, the KH-RT model parameters are carefully adjusted in order to gain an optimised fuel spray secondary breakup. Bearing in mind that the spray flow is highly turbulent, caused by the high injection pressures, it is henceforth considered suitable to calibrate the break-up length (CL). According to the results obtained in Fig. 4, CL value of 7 deviates from the model prediction pattern and underestimates the penetration length. However, CL value of 10 gives acceptably accurate perditions over the entire simulated flow time. Meanwhile, other KH-RT breakup model parameters namely B0 and B1 were left unchanged to their default values, while Ctau and CRT were

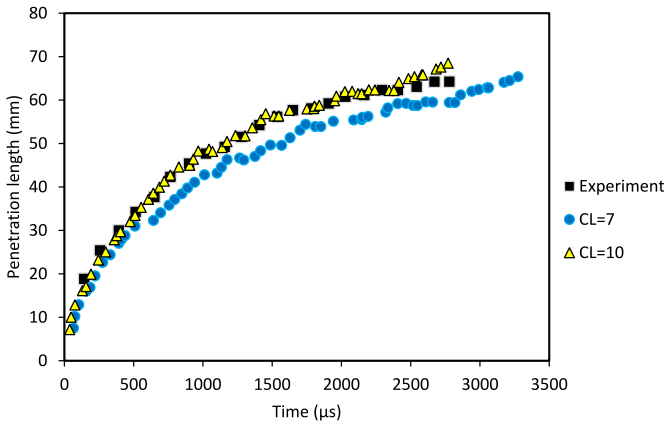

Fig. 4. Spray penetration length of D100 and experimental data [25] versus the break up model constant.

kept at 1 and 0.1 as recommended in the literature [44].

Furthermore, throughout the model setup in Fluent, the wall types are chosen as reflect model, while the SIMPLE method has been used at the commencement of the simulation and once the convergence is reached, it is switched to the coupled method. As for the spatial discretisation of the associated parameters, the second order upwind approach is used to ensure high accuracy of the results [45]. Moreover, since the under-relaxation factors (URF) are quite important to achieve a sustained convergence, a set of trial and error is applied to meticulously detect the optimum values. This is especially the case for the turbulence parameters as it was found that values more than 0.8 could violate the solution convergence due to the high turbulent condition of the model. Meanwhile, the Courant number has also been carefully checked to be within an acceptable range of <0.7 [19,21]. Also, in order to account for the Arrhenius rate as well as the mixing rate, the finite-rate/eddy-dissipation method is used for turbulence-chemistry integration (TCI) in the species module [19]. The volumetric option is employed for the reactions module and given the complexities associated with the chemistry of the integrated fuels and kinetic mechanism, the *relax to chemical equilibrium* mode is integrated for the chemistry solver [19]. Important species involved in the spray-flame development of each fuel are also selected in the reported residual section to inspect the accuracy of the results while simulating. In order to warrant the best solution outcomes, 1E-6 is defined as the convergence criteria for the energy, while 1E-5 was used for other residuals. Bearing in mind the complexities involved for such models, 80 iterations were chosen per time-step to ensure appropriate convergence of the equations.

4.3. Chemical kinetic mechanism

With the improvements attained in the detailed chemical kinetic mechanisms to replicate the combustion characteristics of diesel, biodiesel and gasoline fuels, it is therefore imperative to select a mechanism that is computationally manageable to be used in Fluent simulations. As stated earlier, our research group has proposed a novel multicomponent kinetic mechanism (CDBG mechanism) capable of accurately emulating the ignition behaviour of diesel/biodiesel/gasoline fuels and their mixtures [2]. In our published work, n-heptane was used as diesel surrogate, MB and MD as biodiesel surrogates, and iso-octane and toluene as gasoline surrogates. The surrogates were then reduced using Directed Relation Graphs (DRG) and Directed Relation Graph with Error Propagation (DRGEP) approaches. Then, the reduced mechanisms were merged to form a multicomponent kinetic mechanism. Later, two important analytical tools namely cross-reactions analysis and the Arrhenius reaction rate constants optimisation method were applied on the multicomponent mechanisms to further improve the emulating ability of the mechanism [46]. Afterwards, extensive validation process was investigated to further ascertain the reliability of the proposed mechanism where the results of ID timing, flame speed and species mole fraction were benchmarked against experimental data. The outcomes revealed great correspondence of CDBG mechanism with experimental data. Further information about our recently published work could be found in the literature [2]. Henceforth, in this study the multicomponent CDBG mechanism is utilised to simulate the spray/flame development and soot formation of the respective fuels and their mixtures.

4.4. Soot model

The utilised kinetic CDBG mechanism was equipped with the necessary PAH sub-mechanisms to further elucidate the complexities associated with the soot formation and describe the production and growth of PAHs up to pyrene (A4). The self-amalgamation of propargyl (C_3H_3) radicals can lead to the formation of the simplest aromatic species benzene (A1), while the increment of PAHs species beyond A1 is generally assigned to the H-abstraction/addition of C_2H_2 or C_4H_4 species. For instance, the soot pollutants encompassing C_2H_2, form through several stages as given below [8,47,48]:

$$A4 \rightarrow 16C(s) + 5H_2 \quad (1)$$

$$C(s) + C_2H_2 \rightarrow 3C(s) + H_2 \quad (2)$$

$$nC(s) \rightarrow C(s)_n \quad (3)$$

$$C(s) + \frac{O_2}{2} \rightarrow CO \quad (4)$$

$$C(s) + OH \rightarrow CO + \frac{H_2}{2} \quad (5)$$

in which, Eqns. (1)–(5) account for the soot inception, soot precursors' (C_2H_2 & C_2H_4) surface growth, coagulation, O_2 oxidation and OH oxidation, respectively. It is worthy to mention that when soot particles are formed, they can either increment in mass and size via the surface growth and coagulation processes. Then, the soot oxidation takes place using the Fenimore-Jones oxidation model (as given in the soot module of Fluent). As for the turbulent interaction model in the soot model, the temperature PDF mode is used and default values are used for other model parameters. A summary of the numerical setups is presented in Table 3. It is to be noted that the pressure-velocity scheme was selected as SIMPLE in the commencement of the simulation with first order discretisation schemes. This is to ensure appropriate convergence of the model at the start of the running, and then once the simulation outcomes are converged, the model settings are gently switched to coupled with second high order discretisation.

5. Results and discussion

In this section, the model outputs are extensively validated with experimental data found in the literature in terms of spray development, lift-off length, ignition delay timing and soot formation. Then the simulation outcomes for flame structure, soot formation and emission gases are discussed.

5.1. Model validation

5.1.1. Spray development

Prior to simulating the model and applying the intended setups, it is imperative to validate the accuracy and reliability of the model. To this end, non-evaporating spray in conjunction with reacting spray are benchmarked against the experimental data [24–26]. Spray development, flame LOL, ignition delay (ID) and soot formation were chosen as the benchmarking criteria to validate the current study's outcomes. However, it must be noted due to the lack of reported experimental data

Table 3
Summary of the numerical setups.

Terminology	Particulars
Fluid flow behaviour	Transient mode
Viscosity	Detached Eddy Simulation model (DES)
Spray breakup phenomenon	Kelvin–Helmholtz–Rayleigh–Taylor (KH-RT) model
KH-RT model parameters	CL = 10 | B0 = & B1 = default | Ctau = 1 | CRT = 0.1
Drag phenomenon	Dynamic-Drag model
Turbulence-Chemistry Integration (TCI)	Finite-Rate/Eddy-Dissipation method
Reactions module	Volumetric approach
Chemistry solver	Relax to Chemical Equilibrium mode
Soot formation phenomenon	Moss-Brookes soot model
Soot oxidation phenomenon	Fenimore-Jones oxidation model
Turbulent interaction model in soot module	Temperature PDF mode
Mesh structure	Adaptive mesh refinement (AMR)
Mesh refinement level	5
Wall type	Reflect mode
Pressure-Velocity coupling scheme[a]	SIMPLE | coupled
Spatial discretisation	Second Order Upwind Mode
Transient formulation	Bounded Second Order Implicit
Convergence criteria	Energy = 1E-6 | others residuals = 1E-5
Time-step size	1 μs
Maximum iterations	80[b]

[a] SIMPLE approach is used at first until appropriate convergence is achieved, then the solver is switched to coupled mode.
[b] This number has been given to ensure the convergence is properly achieved.

for non-evaporating spray characteristics of G50BD50, the results of G70BD30 were then employed to serve the purpose. To begin with, as it is portrayed in Fig. 5, the spray development pattern has been well emulated for all the D100, BD100 fuels and G70BD30 mixture. As for D100 and G70BD30, great matching in spray development shape is achieved. Another reason behind the accuracy of the spray development pattern can be the integration of a comprehensive set of robust physicochemical properties as declared earlier.

Additionally, the results of spray penetration length for D100, BD100 and G70BD30 versus the increment of temperature and flow time are presented in Fig. 6. It can be perceived that the spray liquid phase penetration length has been well replicated by the model for all the integrated fuels. Concisely, as for D100 and BD100 great correspondences were obtained, as such the results could fit in an error bar of 9% and 4%, respectively. However, the predicted penetration length for G70BD30 is found to be relatively more deviated compared to BD100 and D100. To be more exact, as the flow time grows, the model overpredicts the penetration length and the results could get errors as high as 11%. Yet, it can still be deemed acceptable and this error might have been imposed due to the differences in the physicochemical properties of the biodiesel and gasoline, and further investigation in this case can be promising.

5.1.2. Flame lift-off length

The computationally achieved results of this study for flame LOL are also validated against experimental data in Fig. 7. A schematic of the liquid length and lift-off length is portrayed in Fig. 7(a), in which the difference between these two lengths is assumed as D-value (as given in Fig. 7(b)). In the experimental procedure, the flame LOL has been measured using the OH chemiluminescence method [24], whereas, in this modelling, the axial distance from the injecting nozzle to the point in which OH mass fraction reaches 2% of its highest amount is used to detect the flame LOL [8]. Another way to do so would be plotting the temperature on the surface of the chamber along the X-axis, and once the spray ignites the temperature data takes a sharp gradient in the vicinity of the ignition. Similarly, one can monitor important species which are either being consumed or produced, in this case, O_2 mass fraction can be used. As such, the location where the flame has started to develop indicates a sharp reduction in the O_2 concentration compared to other locations on the axis. However, it is important to monitor the above variables on both axes. In other words, the flame propagates in both horizontal and vertical directions, therefore, the data for each axis can be retrieved and plotted using other software to accurately measure the flame length and flame height.

It can be inferred from the results that the D-value pattern has been well predicted in regard to the experimental values for all the tested fuels under low and high ambient oxygen levels. Nevertheless, it can be seen that the D-values of the D100 at O_2 = 20% is slightly overpredicted, whilst this value for G70BD30 is marginally underpredicted. This matter could be assigned to different factors e.g. spray break-up parameters or physiochemical properties, yet it is still acceptably in good agreement with experimental data.

5.1.3. Ignition delay and soot formation

The computed ID timing and the soot formation in this study are also compared to experimental data in the literature as presented in Fig. 8. To begin with, in case of the ID timing the average vertex temperature over the chamber surface has been plotted versus the flow time. Once the first cool flame starts to generate, there is a sharp increase in the average surface temperature, which is assigned to the ignition delay time. Furthermore, the average of produced soot mass has been recorded versus flow time throughout the simulation. The predicted ID timings in Fig. 8(a) are accurately close to the experimental values for both low and high ambient O_2 contents. Likewise, the replicated soot production in Fig. 8(b) is in good agreement with experimental values with errors less than 15%.

Bearing in mind that the model validation has shown promising reliability and accuracy in emulating the spray development, flame LOL, ID timing and soot formation, it could be inferred that the model is ready to be used under various fuelling combinations and operating conditions. Therefore, the following sections are dedicated to meticulously analyse the combustion-related phenomena of diesel, biodiesel, gasoline fuels and their mixtures, entailing the flame structure, equivalence ratio, O_2 consumption, soot formation and produced emission gases. However, it is important to note that in the following sections it is tried to keep the blending ratios close to the standards that are currently being implemented in reality (industrial sectors). In other words, although there are numerous investigations to amalgamate biodiesel and gasoline (as well as other additives) with diesel fuel, the combustion behaviour of these additives has not been yet thoroughly scrutinised. Thus, they are being utilised in a smaller proportion than what was applied in above sections, and diesel is likely to remain as the base fuel [49]. For instance, Malaysia has been planning to incorporate 20% of biodiesel within the transportation sector by 2020 [50,51], whilst, recently there has been very limited attempts to integrate gasoline as an additive to counteract the possible downsides of diesel-biodiesel mixtures [52,53]. Given the abovementioned facts, in this study the combustion-related features of D75|BD20|G5, D70|BD20|G10 and D65|BD20|G15 have been analysed and compared to D100 and BD100. It must be pointed out that in the ternary mixtures the biodiesel has been kept with 20% of mole fraction, while the proportions of gasoline and diesel go trade-off. Also, the addition of gasoline is deemed as a tricky part, as the combustion and engine performance are found deteriorating upon a certain level of gasoline addition [54]. Hence, gasoline fractions of 5%, 10% and 15% have been integrated. The results of the simulations are presented in the following parts.

5.2. Flame structure

Fig. 9 portrays the flame structure of the integrated fuels at 2 ms after the start of injection for ambient O_2 concentrations of 15% and 21%, and ambient temperatures of 900 K and 800 K. The reason for choosing t = 2 ms after the injection is that according to the spray development pattern

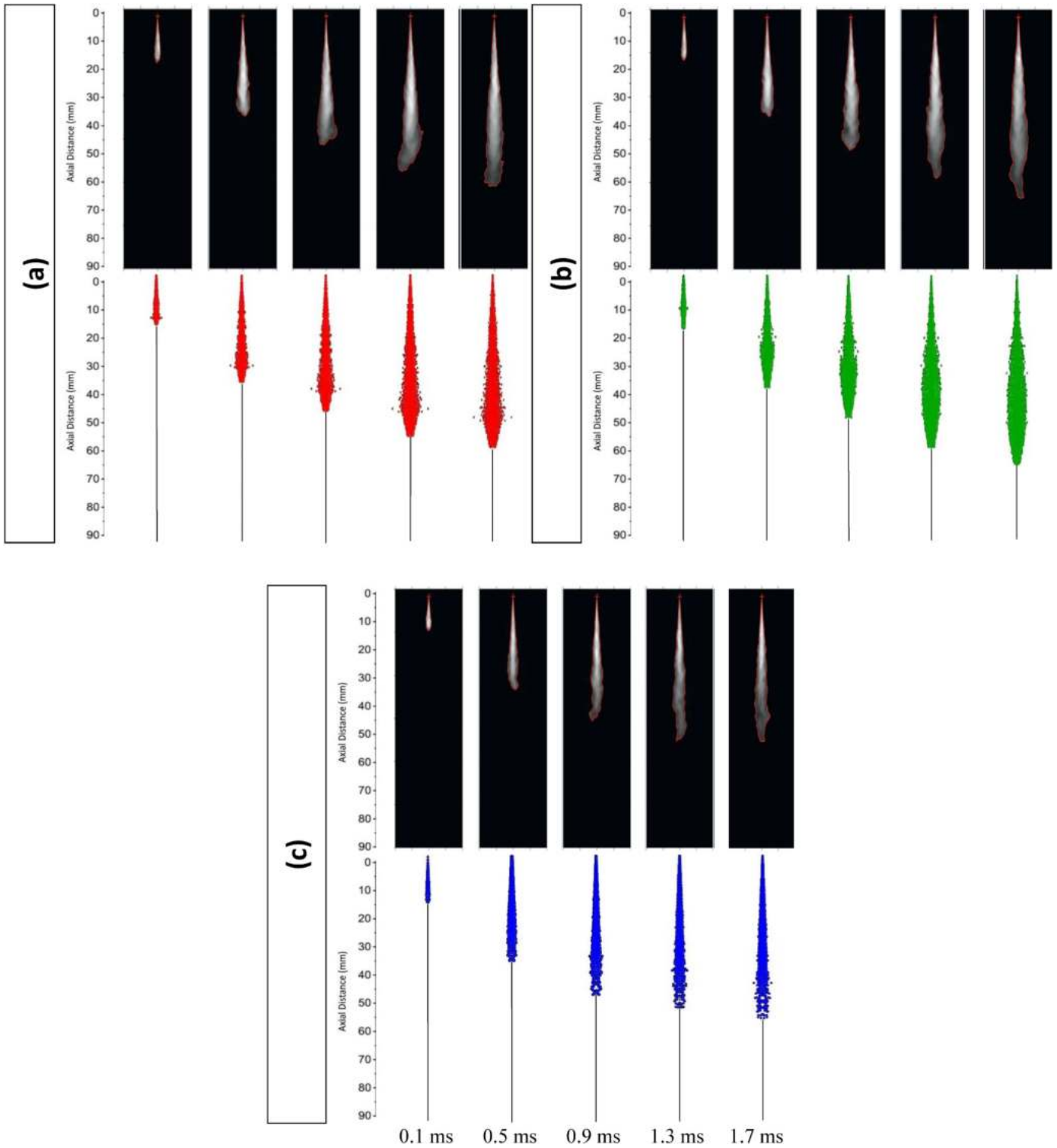

Fig. 5. The spray liquid phase development of (a): D100, (b): BD100, (c): G70BD30 and experimental data [24–26] versus the flow time.

presented in Fig. 6, the spray propagation for the integrated fuels reaches a sustained level at the vicinity of 2 ms, at which the fuel and air are well-mixed, and combustion could have taken place. Subsequent to this time, the flame was further inclined to touch the adjacent walls, which raises the wall impingement effects. Since the comparison here is solely on the combustion-related features of the tested fuels, this phenomenon is avoided as much as possible. Furthermore, the combustion characteristics are analysed under ambient conditions of 800 K and 900 K, and the reason for choosing these two temperatures traces back to the in-cylinder temperatures of actual engines right before the combustion takes place. The effects of varying ambient temperatures on the combustion behaviour of different fuels are well-recognised [9,55,56], and even more so in compression ignition engines whereby the in-cylinder temperature rises up to high values within the 800–900 K range prior to the ignition [8,57,58]. This temperature range roughly remains the same for those regions which have no flame propagation. Therefore, the approximated lowest and highest in-cylinder temperatures (or ambient temperatures), 800 K and 900 K in this work, are fully analysed to

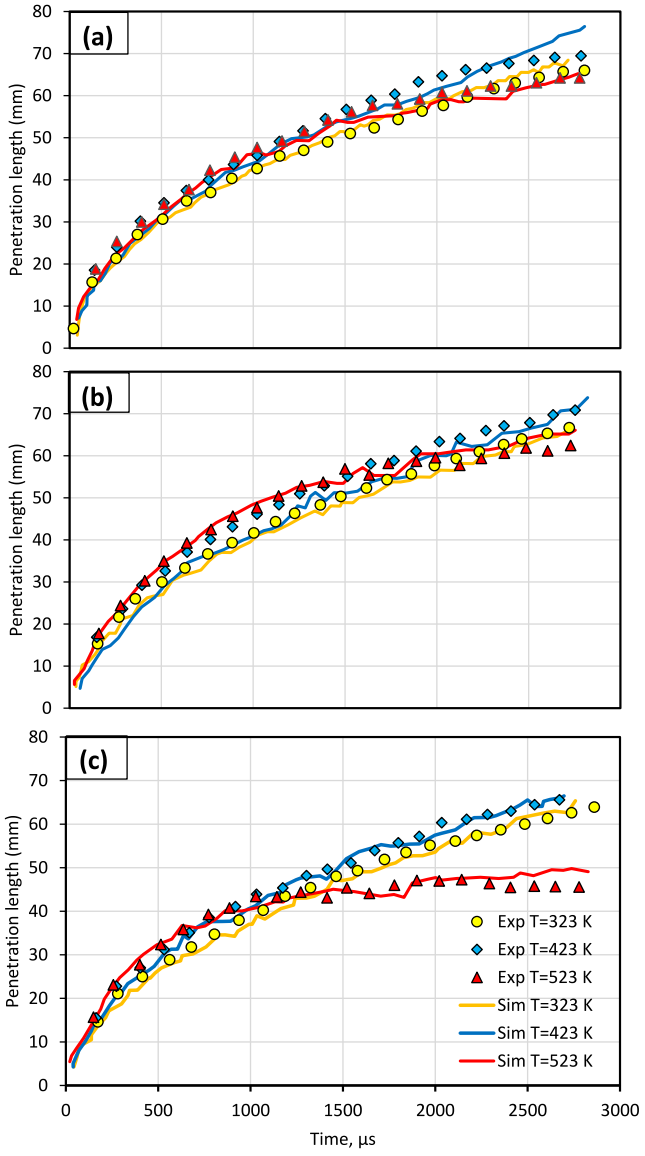

Fig. 6. The comparison between the penetration length of simulated (Lines) (a): D100, (b): BD100, (c): G70BD30 and experimental data (Square markers) [24–26] versus the flow time.

specifically determine the optimum scenario under which the combustion-related features are beneficial.

The dimensions in each of the contour images are 90 × 40 mm in axial and radial directions, respectively. To begin with, it can be perceived that shorter flame LOL is achieved for BD100 followed by gasoline-added blends and D100 at O_2 = 21% and T = 900 K. The shorter flame LOL of biodiesel is due to their different physicochemical properties, as such the stabilised ignition and flame location is moved adjacent to the nozzle vicinity [1,8,26]. To be more exact, the fuel spray consists of liquid phase, transient liquid-vapour phase and vapour phase as further away from the nozzle. The droplets begin to break up near the nozzle tip, and then fuel droplets impact the previously produced droplets and merge with them. It is found that as a result of this amalgamation and droplet collisions, the fuel droplets tend to lose velocity at the jet boundary than the spray axis [55]. The liquid droplets form a cluster in the vicinity of the nozzle tip where no gaseous regimes exist. Further away from this region, a primary droplet break-up takes place producing fuel molecules. In this zone, the interior core of the regime mainly consists of liquid and the external parts contain liquid-gas

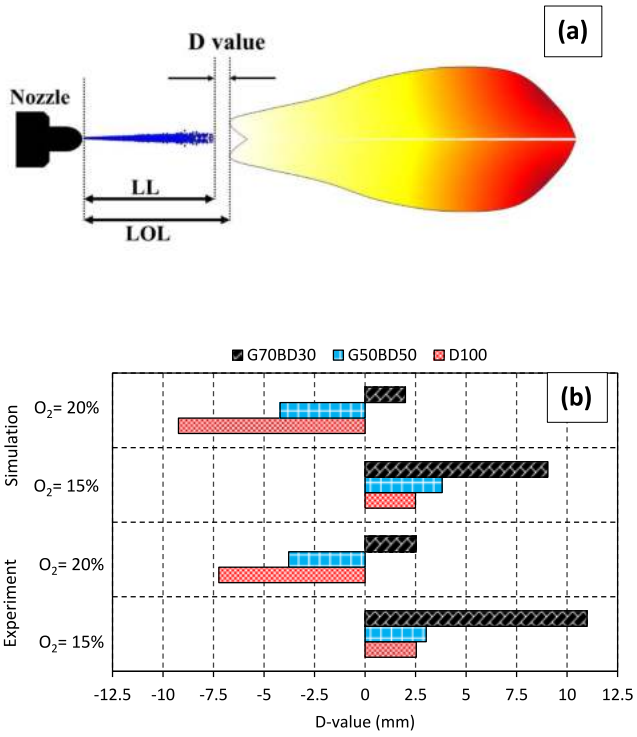

Fig. 7. The (a): schematic of the LL and LOL and the (b): D-values of the simulated D100, G50BD50 and G70BD30 compared with experimental data [24].

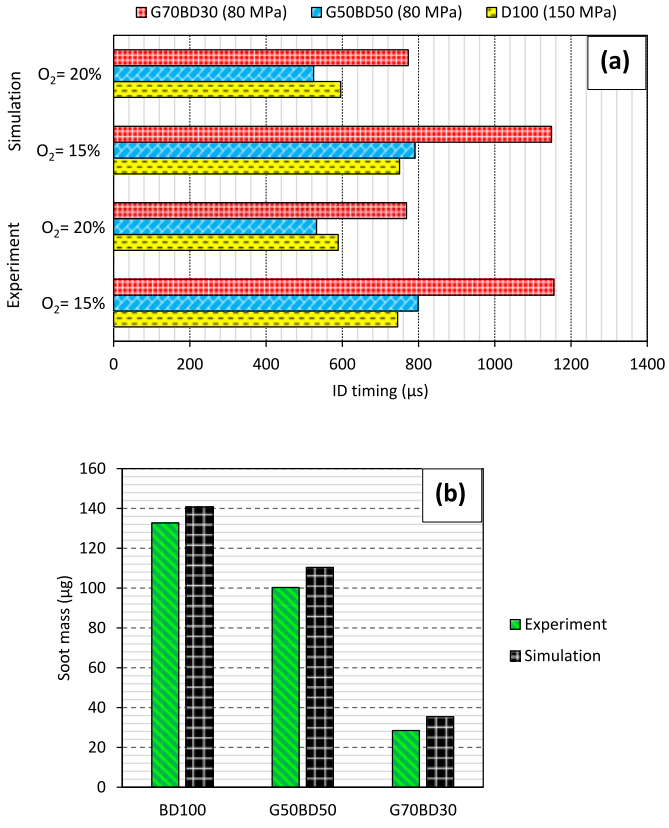

Fig. 8. The computed (a): ID timing of D100, G50BD50 and G70BD30 versus experimental values [24] and the predicted (b): soot mass of BD100, G50BD50 and G70BD30 at O_2 = 15% | T = 900 K compared to experimental data [26].

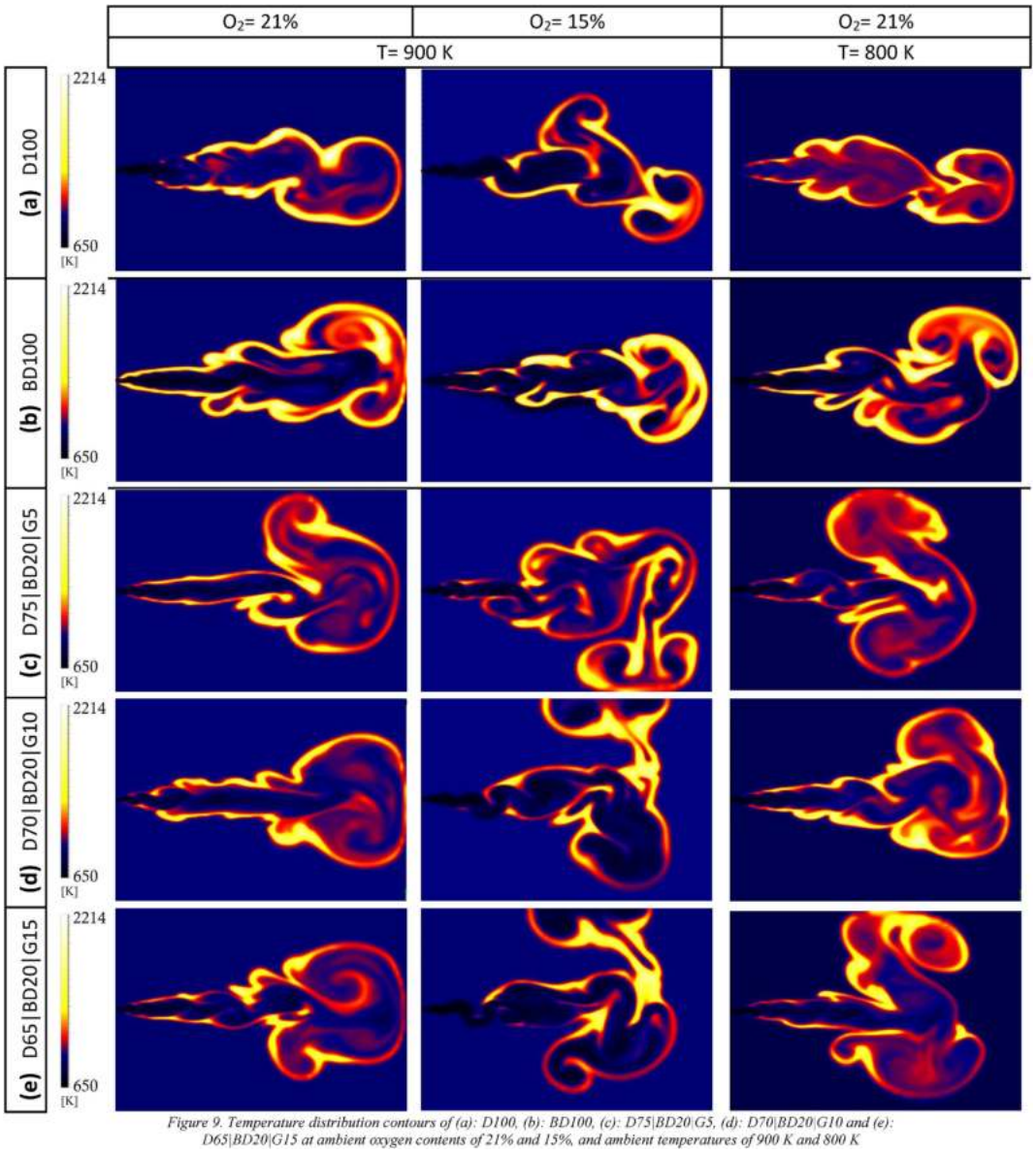

Figure 9. Temperature distribution contours of (a): D100, (b): BD100, (c): D75|BD20|G5, (d): D70|BD20|G10 and (e): D65|BD20|G15 at ambient oxygen contents of 21% and 15%, and ambient temperatures of 900 K and 800 K

Fig. 9. Temperature distribution contours of (a): D100, (b): BD100, (c): D75|BD20|G5, (d): D70|BD20|G10 and (e): D65|BD20|G15 at ambient oxygen contents of 21% and 15%, and ambient temperatures of 900 K and 800 K.

transfer part. Subsequent to the primary break-up region, a huge number of smaller droplets are formed, which depends on the density, viscosity, surface tension, vapour diffusivity, vapour viscosity, pressure, etc. [55,56]. In addition, biodiesel is found to have a wider spray cone angle, which improves air/fuel mixing process with the increased fuel turbulence. Apart from that, as portrayed earlier in Fig. 5, the spray penetration length of diesel is higher than that of biodiesel, which makes the ignitable vapour phase of the flame to be placed further down the stream and increases the LOL. Hence, as calculated earlier in Fig. 1, the combination of these physicochemical properties such as lower vapour viscosity and higher vapour diffusivity of biodiesel compared to diesel results in biodiesel exhibiting a shorter LOL. Additionally, the piston geometry, injection pressure and injection temperature also affect flame LOL, but their effects are not taken into account since they are identical for the tested fuels.

Furthermore, it can be discerned that in all the integrated fuelling scenarios by the increment of the ambient oxygen content the peak of flame temperature increased, with a relatively more extended area for BD100 and gasoline-amalgamated blends. This distinct difference in the flame temperature can be assigned to the thermal effects in addition to the dilution of the surrounding nitrogen. Given the fact that the reduction in nitrogen content would lead to a reduction in the specific heat capacity [8], it could be concluded that less released heat from the fuels is adsorbed and therefore, flame temperature takes higher values. It is also noticeable that by the increase in gasoline fraction from 5% to 15% at $T = 900\ K \mid O_2 = 21\%$, the high flame temperature regions decrease. This could be assigned to the higher volatility of gasoline, which contributes to lower localised temperature regions adjacent to the spray stream. This is also in-line with the findings accomplished in literature [49,54]. Furthermore, the decrease in ambient oxygen level from 21% to 15% ($T = 900\ K$) has led all the integrated fuels to experience a lengthened LOL with greater effects for D65|BD20|G15. The longer fame LOL of the gasoline-added blends compared to BD100 and D100 could be attributed to the longer ID timing imposed by the increase in gasoline fraction (and lower O_2 concentrations). To further clarify this effect, the calculated ID timings for the tested fuels are listed in Table 4. Given the fact that gasoline has lower reactivity in comparison to biodiesel, the addition of gasoline causes the ID timing to be lengthened [57,58]. In

Table 4
The calculated ignition delay timing for the tested fuels under different ambient conditions.

	Ignition delay (μs)		
	$O_2 = 21\% \mid T = 900$ K	$O_2 = 15\% \mid T = 900$ K	$O_2 = 21\% \mid T = 800$ K
D100	837	1248	1544
BD100	458	682	921
D75|BD20|G5	763	975	1222
D70|BD20|G10	788	1005	1351
D65|BD20|G15	801	1032	1417

other words, a higher cetane number of biodiesel leads to shorter ID timing for biodiesel than that of gasoline. Also, bearing in mind that gasoline possesses high degrees of volatility, it can then swiftly form a combustible mixture. However, gasoline must overcome both physical and chemical ignition delays, in which the first is easily overcome but the latter requires a longer time for the chemical radicals to be sufficiently formed and ignited. This phenomenon is attributed to the lower cetane number of gasoline than biodiesel causing the ID timing to be longer [1,2]. It is to be noted that the higher ID timing of diesel compared to biodiesel does not go against the results obtained in Fig. 8, as the injection pressure for diesel in Fig. 8 was 150 MPa for diesel but in here, all the fuels were injected at 80 MPa. This decrease in the injection pressure increases the ID timing of diesel due to less atomisation and air-fuel mixing at 80 MPa compared to 150 MPa. The extended LOL achieved here is agreeable with the results of Fig. 7(b) as the increase in gasoline causes longer LOL comparatively. This phenomenon is also in agreement with finding reported in the literature [49,54,59].

In addition, the flame LOL is lengthened by the decrease in ambient temperature for BD100 and blend cases, but had fewer effects on D100. One of the accountable reasons lying behind this phenomenon could be the descended air-fuel mixing at lower ambient temperatures, under which ignitable gas formation is comparatively suppressed. Moreover, the reduction in ambient temperature increases the associated reactions' activation energy, which ultimately decelerates the reactions and inhibits the formation of OH radicals. Also, the results show that the flame LOL is shifted away from the nozzle region as the ambient temperature decreases. This phenomenon is mainly caused by the prolonged ID timing by the decrease in ambient temperature, and therefore ample of time/space for the fuel and surrounding air to be mixed [2,60]. This is also consistent with the review performed by Zandie et al. [1], where the lower the ambient temperature leads to the longer the ID timing and consequently the longer the flame LOL. Besides, the high flame temperature zones decrease with the addition of gasoline, which represents longer time required for gasoline amalgamated blends to completely combust. Furthermore, the axial flame length of gasoline-added mixtures is slightly lower than D100 and BD100, particularly at $T = 900$ K $\mid O_2 = 15\%$ and $T = 800$ K $\mid O_2 = 21\%$. This could be attributed to the higher ignitability of gasoline and enhanced viscosity [1], whereas the spray atomisation takes place effectively not far away from the nozzle. In other words, as shown in Fig. 6, gasoline-added mixture could reach to a stable spray penetration condition sooner than D100 and BD100.

5.3. Flame and spray development

To better understand the evolution of the spray with time and the combustion initialisation, the flame and spray development for the gasoline added diesel-biodiesel mixtures under the applied ambient conditions are illustrated in the Supplementary Materials, Figures S1-S3. The time frame of the figures for each fuel is from 500 μs to 1300 μs, and for better visualisation of the phenomena involved, the temperature and velocity vectors (backwards and forwards) are incorporated together. Firstly, in Figure S1 with $O_2 = 21\% \mid T = 800$ K, it is noticeable that by the increase in gasoline fraction from 5% to 15%, the spray cone angle increases, from 32.7° to 39.4°. This matter indicates better fuel vaporisation from the very commencement of the injection when gasoline is introduced to the mixture [61,62]. The increase in spray cone angle variation follows the same scenario for Figures S2 and Figure S3 at $O_2 = 21\% \mid T = 900$ K and $O_2 = 15\% \mid T = 900$ K, except that the spray cone angle decreased by approximately 5% for the tested mixtures once O_2 concentration was suppressed to 15%. This matter can prevent promoted spray vaporisation and cause higher soot mass formation, which will be further explained in later sections. It must be pointed out that the spray cone angle has been defined where the fuel concentration reaches 1e-5 from the axis (both above and below the axis). Furthermore, sufficient air entrapment in the air-fuel mixing process is imperative to achieve a homogenous air-fuel distribution within the chamber and avoid highly rich or highly lean zones, as will be explained in detail in the next section. As the fuel is injected to the combustion chamber, the centre of spray experiences higher velocity (as shown by the velocity vectors) along the axis while the external parts gradually lose acceleration (velocity vectors with low intensity) and since the chamber is pre-filled with air, those low-velocity droplets collide with air molecules and tend to form a vortex shaped circles. These circles are marked in Figure S1 in green arrows where the velocity vectors form a circular shape. It must be noted that to avoid crowded arrow numbers, only a few of these vortexes are marked. These vortexes are expected to initiate the combustion because the spray break-up, vaporisation and mixing with air has sufficiently occurred [63,64]. To be more exact, in Figure S1 as the fuel continues to develop, the first signs of combustion is observed from the external part of the spray cone where the vortexes exist. It is noteworthy to highlight that since gasoline addition gives rise to larger ID timing, the larger combustion zone is firstly formed for D75|BD20|G5, followed by D70|BD20|G10 and D65|BD20|G15. This matter continues to be true as the flame propagates further, as such D75|BD20|G5 reaches a sustained combustion stage (wider flame zone across the spray zone) sooner whilst the other two mixtures are still undergoing ID.

Moreover, as explained earlier, there are three fuel regions existing at the same time after the injection. In the regions near the injector tip, the fuel still retains a liquid phase with the tendency to break up the droplets and form smaller droplets. A little bit further from this region is the liquid-gas transitionary region where the liquid droplets are getting gradually vaporised, and lastly, the well-vaporised spray region is the last zone [55]. When more time is given to the system, the tip of the spray consisting of the fully vaporised sprays tends to move further away from the transitionary zone [65]. How much further this zone can get before combustion is dependent on the fuel physicochemical properties such as vapour diffusivity, vapour viscosity, surface tension, etc. Bearing this in mind, it is noticeable in Figure S1 that the tip of spray tends to get separated from the main spray zone with two vortexes rotating inversely before the combustion, and subsequently, better air-fuel mixing can be achieved in this zone. Also, for D65|BD20|G15, this separation is more visible as the velocity vectors show a sharp reduction in velocity between the separated spray tip and main zone. However, since the D65|BD20|G15 mixture has not yet overcome the ID timing, no sign of combustion (sharp rise in temperature) can be seen for the region between the separated spray tip and the main spray zone while in the meantime the D70|BD20|G10 mixture exhibits first signs of combustion in this zone due to the comparatively shortened ID timing. In addition, the relatively lower ambient temperature in Figure S1 (800 K) must have further suppressed ignition in the spray tip zone. In other words, as can be perceived from Figure S2, the rise in ambient temperature (900 K) has led the D65|BD20|G15 mixture to overcome the extended ID timing and the separated spray tip reveals signs of ignition before other two mixtures. It must be noted that the high-temperature zones in Figures S1-S3 are graphically rendered for better visualisation while Fig. 9 must be used for the flame temperature comparisons.

Conversely, with the reduction in ambient oxygen concentration to

15% (T = 900 K) in Figure S3, it is apparent that the mixtures take a longer time to ignite as explained in the previous section. The clarifications regarding the flame and spray development given above are also true for the phenomena observed here. For example, the D75|BD20|G5 mixture portrays more propagated flame structures as time goes by compared to D70|BD20|G10 and D65|BD20|G15, due to its shorter ID timing. The separation of the spray tip zone is also more apparent with a relatively greater separation for D65|BD20|G15 compared to the other two cases. Nonetheless, the reduction in ambient oxygen concentration in conjunction with the extended ID timing restrict this zone to be ignited as fast as the D75|BD20|G5 case.

5.4. Equivalence ratio and O_2 concentration

Equivalence ratio is defined as the actual fuel/oxidizer ratio per the stoichiometric fuel/oxidizer ratio. The contours of equivalence ratios are given in Fig. 10. The results reveal higher fuel-rich zones for BD100 and D100 compared to gasoline-added mixtures, particularly for spray core zone at T = 900 K | O_2 = 21%. Bearing in mind the fact that gasoline possesses lower viscosity, cetane number and surface tension than biodiesel, promoted fuel-air mixing is feasible to achieve through the entrainment effect [26]. Moreover, higher distributions of equivalence ratio at the spray centre vicinity for the case of O_2 = 15% compared to O_2 = 21% is achieved (T = 900 K). This phenomenon could be attributed to the high concentrated presence of unburnt fuel spray at the spray centre when O_2 level is lowered to 15%, which ultimately results in comparatively higher equivalence ratios. By the decrease in the ambient temperature to 800 K (O_2 = 21%), the equivalence ratios domains became narrower and the peak values reduced sharply, therefore boosted air-fuel mixing is achieved. This is in-line with the results achieved in previous investigations [8,54].

Fig. 11 shows the computed O_2 concentration for the integrated fuels. The results of O_2 spreading is in-line with abovementioned findings. It can be concluded that extended consumption of O_2 concentration represents more spray break-up as well as more air entrainment [8,25]. Therefore, as it can be noticed from the contours, the reduction in ambient oxygen content for the same ambient temperature of 900 K shows higher O_2 presence surrounding the flame vicinity. This regional excess of O_2 indicates poor oxidisation of the fuels, and the formation of rich fuel mixtures with higher unconsumed O_2 as gasoline fraction gave

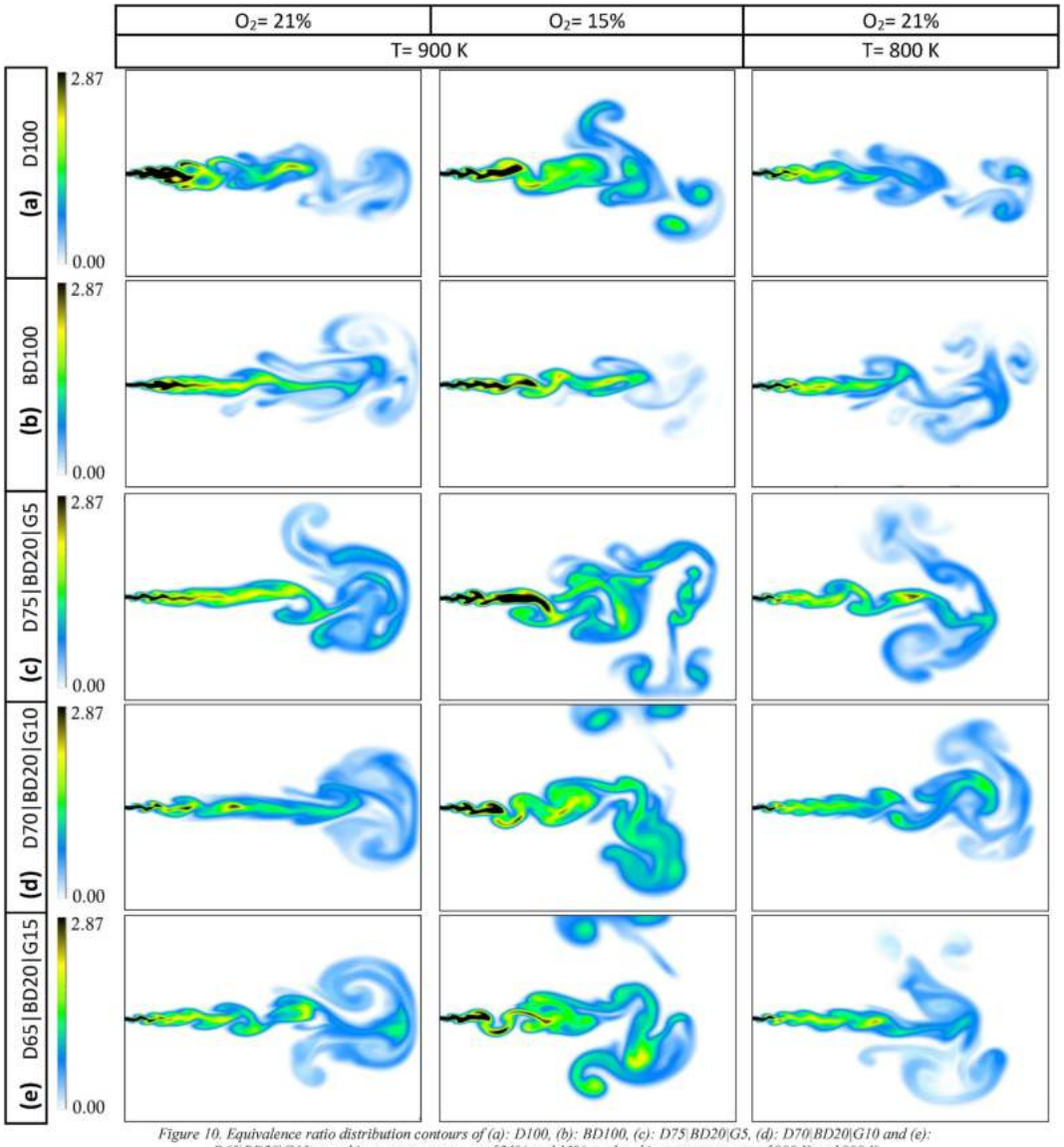

Figure 10. Equivalence ratio distribution contours of (a): D100, (b): BD100, (c): D75|BD20|G5, (d): D70|BD20|G10 and (e): D65|BD20|G15 at ambient oxygen contents of 21% and 15%, and ambient temperatures of 900 K and 800 K

Fig. 10. Equivalence ratio distribution contours of (a): D100, (b): BD100, (c): D75|BD20|G5, (d): D70|BD20|G10 and (e): D65|BD20|G15 at ambient oxygen contents of 21% and 15%, and ambient temperatures of 900 K and 800 K.

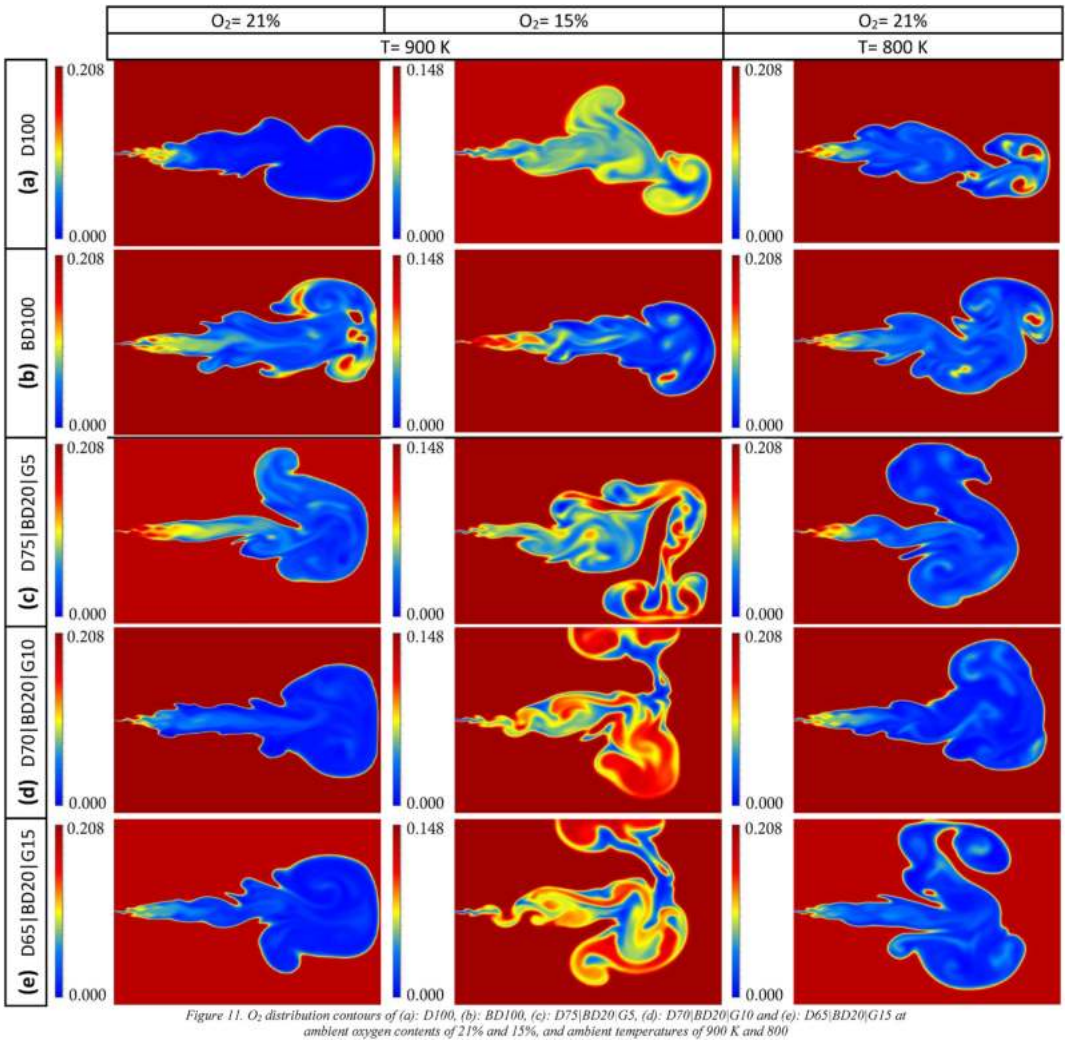

Figure 11. O_2 distribution contours of (a): D100, (b): BD100, (c): D75|BD20|G5, (d): D70|BD20|G10 and (e): D65|BD20|G15 at ambient oxygen contents of 21% and 15%, and ambient temperatures of 900 K and 800

Fig. 11. O_2 distribution contours of (a): D100, (b): BD100, (c): D75|BD20|G5, (d): D70|BD20|G10 and (e): D65|BD20|G15 at ambient oxygen contents of 21% and 15%, and ambient temperatures of 900 K and 800 K.

rise to in the mixture, due to the longer associated ID timing.

5.5. Soot formation

Of the most important species in kinetic mechanisms accountable for controlling the soot growth is C_2H_2 [1,66,67]. The predicated mass fractions of C_2H_2 for BD100, D100 and G50BD50 after 2 ms flow time is shown in Fig. 12(a). According to the results, relatively lower C_2H_2 mass fraction was achieved for T = 800 K | O_2 = 21% with an average (on the tested fuels) relative difference of ~40% and ~55% compared to T = 900 K | O_2 = 21% and T = 900 K | O_2 = 15%, respectively. Furthermore, the produced C_2H_2 decreased with the increase in gasoline fraction in the mixture in all the tested scenarios while BD100 out-produced D100 only at T = 900 K | O_2 = 15%. Nevertheless, more produced PAH species (A4) is achieved for gasoline-added blends compared to BD100 (but slightly less than D100) despite having lower soot surface growth. For further clarity, the computed soot mass and PAHs mass fractions are also given in Fig. 12(b) for the tested fuels under different ambient conditions. This outcome shows the possibility that the soot production might be higher for the gasoline-added mixture compared to BD100. However, this has been ascertained not to be the case. As such, previous researchers attributed this phenomenon to the gasoline's aromatic nature, which is accountable for altering the soot production and PAH species [68,69]. To confirm this hypothesis, in addition to the computed soot mass in Fig. 12(b), the soot mass contours of the tested fuels are plotted in Fig. 13. The contours results indicate that D100 produces higher mass fractions of soot than that of BD100 and gasoline-added mixtures at T = 900 K | O_2 = 21%. In addition, given that LOL is the distance that the fuel penetrates prior to the commencement of high temperature reactions, it can also be concluded that higher soot mass of D100 compared to other cases is due to its extended LOL, as shown in Figs. 7 and 9. In other words, the more the LOL extends, the more air is sucked and subsequently, a leaner mixture will be generated upstream of the LOL [8]. It must be pointed out that since the distribution pattern of A4 under other scenarios were analogous to the trend obtained for the C_2H_2 mass fraction, the A4 mass fraction distributions for other conditions are not presented here.

Moreover, by the reduction of oxygen content from 21% to 15%, the predicted soot mass tends to rise for all the tested fuels. Meanwhile, the most favourable condition is perceived for T = 800 K | O_2 = 21%, where the soot mass for all the modelled fuels has dramatically supressed. One possible explanation for this could be either the reduction in pyrolysis process of fuels or the inhibited formation of soot precursors as reported in a previous study [70]. The study found the pyrolysis process to be highly sensitive to temperature, in which higher temperatures resulted in enhanced pyrolysis process and vice versa. Given the point that flame LOL is more extended upstream at lower ambient temperature, descended fuel-air mixing is expected to happen since flame LOL was

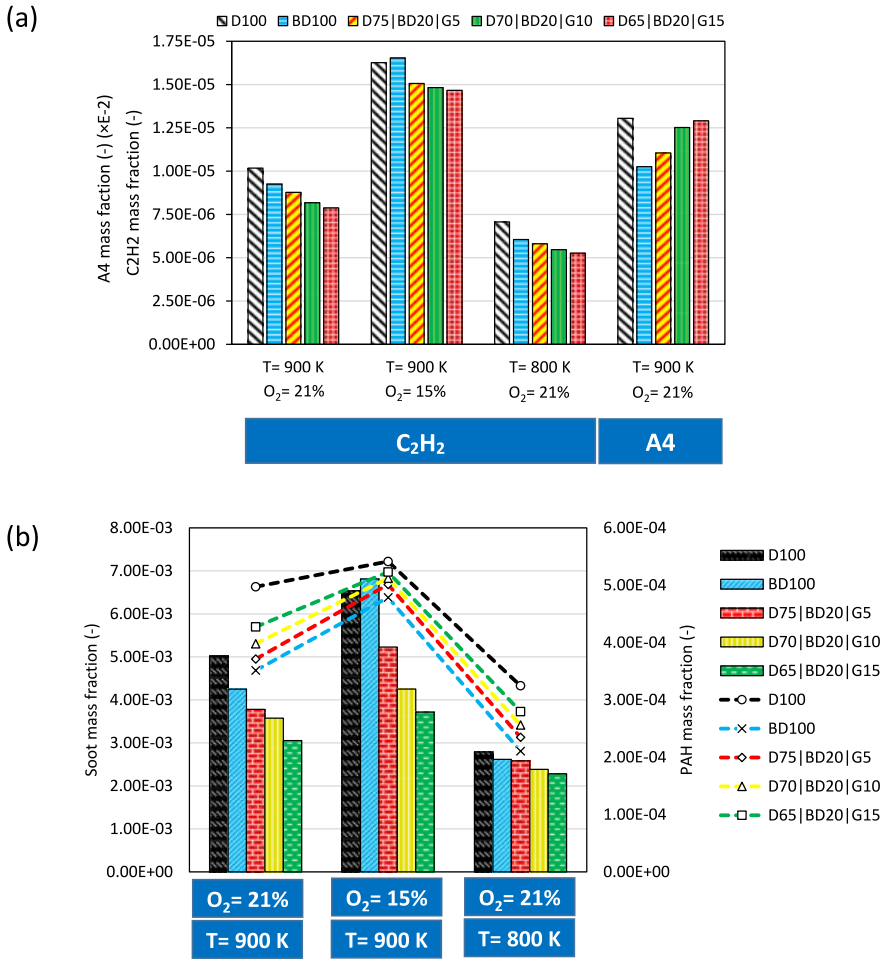

Fig. 12. The predicted (a): C_2H_2 and A4 mass fractions and (b): soot mass and PAHs mass fractions for D100, BD100, D75|BD20|G5, D70|BD20|G10 and D65|BD20|G15 under different ambient conditions.

beneficial to promote the air entrainment phenomenon. This is in-line with the equivalence ratio contours in Fig. 10. Also, the increase in the gasoline content of the mixtures has revealed improving effects in supressing the produced soot mass particularly for D65|BD20|G15.

In addition, since the produced soot mass goes hand in hand with the surface growth affected by C_2H_2, it is important to note that by the increment of oxygen content more C_2H_2 is consumed through the reactions as below:

$$C_2H_2 + OH = CH_2CO + H \quad (6)$$

$$O_2 + C_2H_2 = CO + CH_2O \quad (7)$$

$$C_2H_2 + O = OH + C_2H \quad (8)$$

$$O_2 + C_2H_2 = HO_2 + C_2H \quad (9)$$

therefore, since the surface growth plays a significant role in the total produced soot mass [8], higher consumption of C_2H_2 leads to lower soot mass formation by the raise in ambient oxygen level. On the other hand, under low ambient temperature condition (T = 800 K), the C_2H_2 species tend to form slower through the associated reactions as below [8]:

$$C_2H_4(+M) = C_2H_2 + H_2(+M) \quad (10)$$

$$C_2H_3 + H = C_2H_2 + H_2 \quad (11)$$

$$C_2H_3 + OH = C_2H_2 + H_2O \quad (12)$$

$$C_3H_2 + OH = C_2H_2 + HCO \quad (13)$$

which subsequently lower soot mass is produced as the ambient temperature decreases.

5.6. Exhaust emissions

The predicted values of emission gases comprising NO_x, CO_2 and CO for D100, BD100, D75|BD20|G5, D70|BD20|G10 and D65|BD20|G15 after 3 ms of flow time are presented in Fig. 14. The results of NO_x emissions in Fig. 14(a) is the sum of produced NO_2 and NO species, whereas N_2O, N_2O_3 and N_2O_5 species are usually neglected [71]. It must be pointed out that the NO_x give-outs behaviour in oxygenated fuel blends is deemed as complex phenomena and not conclusive [1,49,54]. The results reveal that B100 forms higher NO_x mass fractions for all the tested scenarios compared to D100, with the highest relative difference of ~50% at T = 900 K | O_2 = 15%. NO_x formation is mainly controlled by the reaction time, adiabatic flame temperature and the oxygen concentration [49,54]. This could be the reason lying behind the higher formed NO_x mass fraction for BD100 than D100. On the other hand, lower NO_x emissions are achieved as the gasoline fraction increases in the mixture, nevertheless, still higher than D100. This could be taken up on different levels. First, the addition of gasoline to biodiesel-diesel reduces the chamber combusting temperature, as portrayed schematically in Fig. 9, as well as the decrease in cetane number [49,71]. Besides, addition of gasoline will bring about extended ID timing as illustrated in

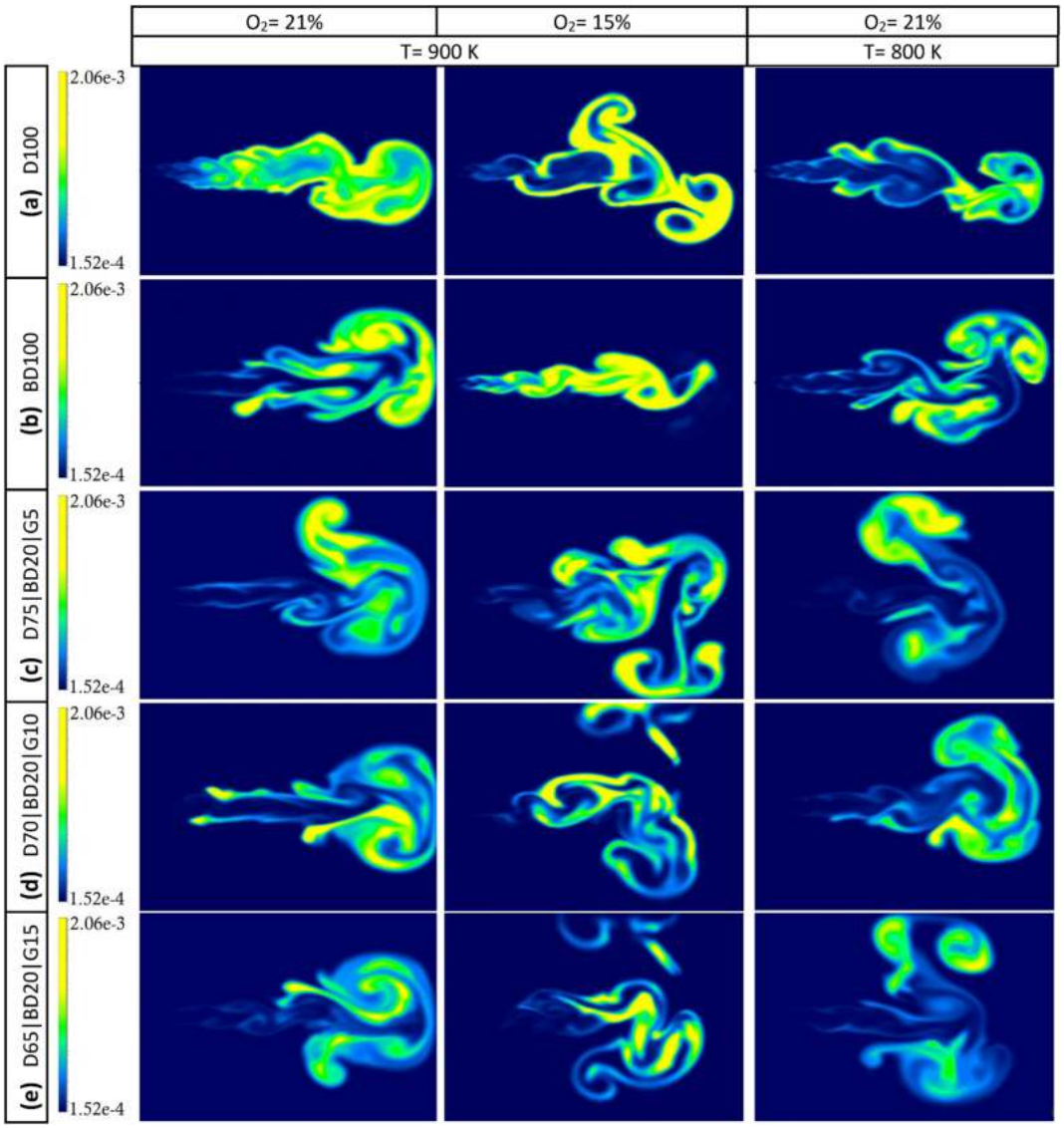

Fig. 13. Soot mass fraction distribution contours of (a): D100, (b): BD100, (c): D75|BD20|G5, (d): D70|BD20|G10 and (e): D65|BD20|G15 at ambient oxygen contents of 21% and 15%, and ambient temperatures of 900 K and 800 K.

Fig. 8(a), thus, the premixed combustion mode will be greater for gasoline-added mixtures compared to BD100 [71,72]. It has also been ascertained that lower combustion duration of gasoline-added blends compared to BD100 could lead to lower NO_x formation of gasoline-biodiesel blends in comparison to pure biodiesel [1,49,54]. The combination of abovementioned phenomena causes the increased gasoline fraction to engender lower NO_x mass fractions.

Furthermore, according to the produced CO_2 emissions in Fig. 14(b), D100 brought about higher CO_2 mass fractions comparatively for the all the tested scenarios. Bearing in mind that BD100 contain higher O_2 molecules in their structure, less O_2 is required compared to D100 throughout the combustion. In other words, the higher O_2 and H molecules present in the fuel structure, the lower the CO_2 emissions [73]. Also, the addition of gasoline has revealed slightly lower CO_2 emissions. Moreover, the results of CO emissions in Fig. 14(c) indicate that BD100 produced lower CO mass fractions compared to D100. The higher oxygen content found in biodiesels could be accountable for this matter, which results in an enhanced combustion mode and reduced fuel-rich zones (as shown in Fig. 10) [49,54,74–78]. In addition, it has been predicted that adding gasoline to biodiesel-diesel blends causes even greater reduction in CO emissions. Gasoline addition to biodiesel increases the blend volatility, and consequently more extended over-lean zones is achieved within the chamber, which reduces the CO emissions [49,54,71,73].

6. Recommendations for future work

The outcomes of numerical studies such as the current research is highly demanded, simply because there have been serious concerns about the jeopardising effects of fossil fuels utilisation. Therefore, there is an urgent need to meticulously analyse the challenges involve with dual or ternary fuelling strategies, as a promising solution. However, as far as numerical investigations are concerned, there is always room for improvement. Of the most important aspects future works could delve into would be experimental studies, as there is a considerable dearth of data in this regard to be used for numerical works' validation stages. In other words, although the current work has been thoroughly validated prior to performing the tests, it is yet deemed important to scrutinise the outcomes through experimentation, particularly for the ternary mixture of interest here. Moreover, conducting simulations on a 3-D engine model to accurately visualise the hypotheses made here is demanded. One of the important benefits in doing so would be to ascertain the

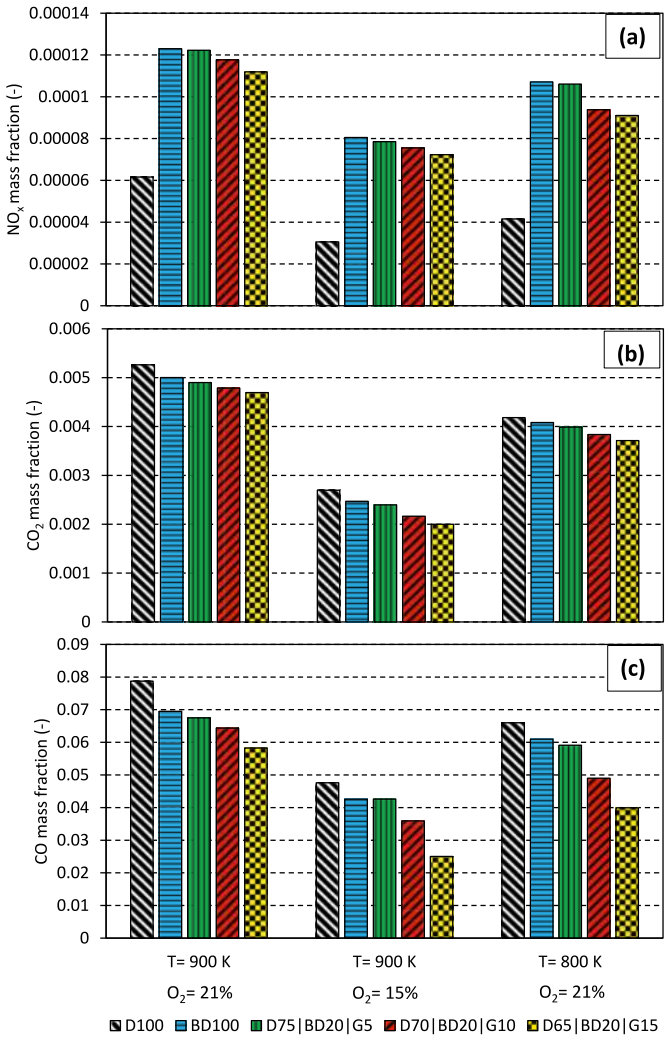

Fig. 14. The predicted (a): NO_x, (b): CO_2 and (c): CO emissions for D100, BD100, D75|BD20|G5, D70|BD20|G10 and D65|BD20|G15 under different ambient conditions.

optimum blending ratio of this ternary fuelling strategy, as it could be better decided with features like heat release rate, pressure trace, specific fuel combustion, thermal efficiency, coefficient of variance, etc.

7. Concluding remarks

The current CFD analysis aims to analyse the spray/flame development, soot formation and emission gases of diesel, biodiesel and biodiesel-gasoline under compression ignition engine-relevant conditions. A compact combined multicomponent kinetic mechanism for diesel-biodiesel-gasoline mixtures that is also equipped with necessary reactions to model soot formation from our recently published work has been incorporated. This study also provides a comprehensive measurement of physicochemical properties encompassing vapour, liquid and critical properties. The results of the simulated models were benchmarked against the experimental data found in literature, in terms of spray liquid penetration length, flame lift-off length, ignition delay and soot formation. The simulations were conducted for diesel, biodiesel and gasoline under dual/ternary blending approaches in a constant volume chamber under different ambient conditions. Following conclusions were drawn:

I. The produced soot mass was relatively greater for D100, where BD100 produced lower values and the addition of gasoline to diesel-biodiesel blend resulted in even greater reduction of produced soot mass.
II. The increase in ambient oxygen concentration from 15% to 21% improved the consumption of soot precursors and decreased PAHs as well as soot formation. This phenomenon was found to be more intense for biodiesel compared to diesel and gasoline-added biodiesel-diesel mixtures.
III. The decrease of ambient temperature was also found significantly influential, as such, lower soot formation was predicted for all the tested fuels when the temperature was reduced from 900 K to 800 K (same O_2 concentration); specifically, the lowest soot mass yield was predicted for D65|BD20|G15 mixture.
IV. Lower nitrogen oxides emissions were achieved for D100 compared to BD100, whilst, the amalgamation of gasoline with diesel-biodiesel blend exhibited lower NO_x emissions compared to BD100, but still higher than D100 comparatively. Contrarily, lower carbon dioxide and carbon monoxide emissions were achieved for gasoline-added diesel-biodiesel mixtures in comparison with D100 and BD100.

Credit author statement

Mohammad Zandie: Methodology, Formal analysis, Visualisation, Writing – original draft. **Hoon Kiat Ng**: Conceptualization, Funding acquisition, Supervision. **Suyin Gan**: Supervision, Writing - Reviewing and Editing. **Mohd Farid Muhamad Said**: Conceptualization, Funding acquisition, Validation. **Xinwei Cheng**: Supervision, Validation.

Declaration of competing interest

The authors declare that they have no known competing financial interests or personal relationships that could have appeared to influence the work reported in this paper.

Data availability

The data that has been used is confidential.

Acknowledgement

The Ministry of Higher Education (MOHE), Malaysia is gratefully acknowledged for the financial support towards this project under the Fundamental Research Grant Scheme FRGS/1/2019/TK03/UNIM/01/1.

Appendix A. Supplementary data

Supplementary data to this article can be found online at https://doi.org/10.1016/j.energy.2022.125191.

References

[1] Zandie M, Ng HK, Gan S, Said MFM, Cheng X. Review of the advances in integrated chemical kinetics-computational fluid dynamics combustion modelling studies of gasoline-biodiesel mixtures. J Transport Eng 2021:100102.
[2] Zandie M, Ng HK, Gan S, Said MFM, Cheng X. Development of a reduced multi-component chemical kinetic mechanism for the combustion modelling of diesel-biodiesel-gasoline mixtures. J Transport Eng 2021:100101.
[3] Zuo L, Wang J, Mei D, Dai S, Adu-Mensah D. Experimental investigation on combustion and (regulated and unregulated) emissions performance of a common-rail diesel engine using partially hydrogenated biodiesel-ethanol-diesel ternary blend. Renew Energy 2022;185:1272–83.
[4] Liaquat A, Masjuki H, Kalam M, Fazal M, Khan AF, Fayaz H, Varman M. Impact of palm biodiesel blend on injector deposit formation. Appl Energy 2013;111:882–93.
[5] Liu Y, Yuan Z, Ma Y, Fu J, Huang R, Liu J. Analysis of spray combustion characteristics of diesel, biodiesel and their n-pentanol blends based on a one-dimensional semi-phenomenological model. Appl Energy 2019;238:996–1009.
[6] Zhong W, Xuan T, He Z, Wang Q, Li D, Zhang X, Huang YY. Experimental study of combustion and emission characteristics of diesel engine with diesel/second-generation biodiesel blending fuels. Energy Convers Manag 2016;121:241–50.

[7] Xuan T, Cao J, He Z, Wang Q, Zhong W, Leng X, Li D, Shang W. A study of soot quantification in diesel flame with hydrogenated catalytic biodiesel in a constant volume combustion chamber. Energy 2018;145:691–9.
[8] Zhong W, Mahmoud NM, Wang Q. Numerical study of spray combustion and soot emission of gasoline–biodiesel fuel under gasoline compression ignition-relevant conditions. Fuel 2022;310:122293.
[9] Xu S, Zhong S, Pang KM, Yu S, Jangi M, Bai X-s. Effects of ambient methanol on pollutants formation in dual-fuel spray combustion at varying ambient temperatures: a large-eddy simulation. Appl Energy 2020;279:115774.
[10] Zhong S, Xu S, Bai X-S, Peng Z, Zhang F. Large eddy simulation of n-heptane/syngas pilot ignition spray combustion: ignition process, liftoff evolution and pollutant emissions. Energy 2021;233:121080.
[11] Zhang Z, Tian J, Xie G, Li J, Xu W, Jiang F, Huang Y, Tan D. Investigation on the combustion and emission characteristics of diesel engine fueled with diesel/methanol/n-butanol blends. Fuel 2022;314:123088.
[12] Kuti OA, Sarathy SM, Nishida K. Spray combustion simulation study of waste cooking oil biodiesel and diesel under direct injection diesel engine conditions. Fuel 2020;267:117240.
[13] Pischke P, Christ D, Cordes D, Kneer R. Application of detached eddy simulation to Lagrangian spray simulations. 2014.
[14] Sehole HAH, Riaz R, Maqsood A. Detached eddy simulation of turbulent spray combustion in a turbo jet combustor-prediction of NO_x concentration. In: AIAA SCITECH 2022 Forum; 2022.
[15] Zhang M, Ong JC, Pang KM, Bai X-S, Walther JH. An investigation on early evolution of soot in n-dodecane spray combustion using large eddy simulation. Fuel 2021;293:120072.
[16] Mishra K, Das MK, De A, Kar KK. Hybrid RANS/LES simulation of methane–LO_x combustion. In: Sustainable development for energy, power, and propulsion. Springer; 2021. p. 199–219.
[17] Shin J, Sung H-G. Combustion characteristics of hydrogen and cracked kerosene in a DLR scramjet combustor using hybrid RANS/LES method. Aero Sci Technol 2018;80:433–44.
[18] Chaouat B. The state of the art of hybrid RANS/LES modeling for the simulation of turbulent flows. Flow, Turbul Combust 2017;99(2):279–327.
[19] Fluent A. R2 User's guide. ANSYS Inc.; 2019.
[20] Shu J, Fu J, Liu J, Ma Y, Wang S, Deng B, Zeng D. Effects of injector spray angle on combustion and emissions characteristics of a natural gas (NG)-diesel dual fuel engine based on CFD coupled with reduced chemical kinetic model. Appl Energy 2019;233:182–95.
[21] Zandie M, Kazemi A, Ahmadi M, Moraveji MK. A CFD investigation into the enhancement of down-hole de-oiling hydro cyclone performance. J Pet Sci Technol 2021;199:108352.
[22] Du W, Zhang Q, Zhang Z, Lou J, Bao W. Effects of injection pressure on ignition and combustion characteristics of impinging diesel spray. Appl Energy 2018;226:1163–8.
[23] Shang W, He Z, Wang Q, Cao J, Li B, Leng X, Tamilselvan P, Li D. Experimental and analytical study on capture spray liquid penetration and combustion characteristics simultaneously with Hydrogenated Catalytic Biodiesel/Diesel blended fuel. Appl Energy 2018;226:947–56.
[24] Zhong W, Li B, He Z, Xuan T, Lu P, Wang Q. Experimental study on spray and combustion of gasoline/hydrogenated catalytic biodiesel blends in a constant volume combustion chamber aimed for GCI engines. Fuel 2019;253:129–38.
[25] Yuan W, Liao J, Li B, Zhong W. Experimental study on spray characteristics of gasoline/hydrogenated catalytic biodiesel under GCI conditions. Chemistry 2020:2020.
[26] Zhong W, Xiang Q, Pachiannan T, Mahmoud NM, Li B, He Z, Wang Q, Sun J. Experimental study on in-flame soot formation and soot emission characteristics of gasoline/hydrogenated catalytic biodiesel blends. Fuel 2021;289:119813.
[27] Payri R, Gimeno J, Cardona S, Ayyapureddi S. Experimental study of the influence of the fuel and boundary conditions over the soot formation in multi-hole diesel injectors using high-speed color diffused back-illumination technique. Appl Therm Eng 2019;158:113746.
[28] Ismail HM, Ng HK, Cheng X, Gan S, Lucchini T, D'Errico G. Development of thermophysical and transport properties for the CFD simulations of in-cylinder biodiesel spray combustion. Energy Fuel 2012;26(8):4857–70.
[29] Cheng X. Development of reduced reaction kinetics and fuel physical properties models for in-cylinder simulation of biodiesel combustion. University of Nottingham; 2016.
[30] Reid RC, Prausnitz JM, Sherwood TK. The properties of gases and liquids. New York: McGraw-Hill; 1977.
[31] Lin R, Tavlarides LL. Thermophysical properties needed for the development of the supercritical diesel combustion technology: evaluation of diesel fuel surrogate models. J Supercrit Fluids 2012;71:136–46.
[32] Cragoe CS. Therm Prop Petrol Prod: November 1929;9. 1929.
[33] Naziev YM, Aliev M, Efendiev V. Thermophysical properties of A-72 gasoline at various temperatures and pressures. Chem Technol Fuels Oils 1974;10(8):626–8.
[34] Ra Y, Reitz RD, McFarlane J, Daw CS. Effects of fuel physical properties on diesel engine combustion using diesel and bio-diesel fuels. SAE Int J Fuels Lubr 2009;1(1):703–18.
[35] Chakravarthy K, McFarlane J, Daw S, Ra Y, Reitz R, Griffin J. Physical properties of bio-diesel and implications for use of bio-diesel in diesel engines. SAE Trans 2007:885–95.
[36] Reid RC, Prausnitz JM, Poling BE. The properties of gases and liquids. 1987.
[37] van Bommel MJ, Oonk HA, van Miltenburg JC. Heat capacity measurements of 13 methyl esters of n-carboxylic acids from methyl octanoate to methyl eicosanoate between 5 K and 350 K. J Chem Eng Data 2004;49(4):1036–42.
[38] Allen CA, Watts K, Ackman R, Pegg M. Predicting the viscosity of biodiesel fuels from their fatty acid ester composition. Fuel 1999;78(11):1319–26.
[39] Yuan W, Hansen A, Zhang Q. Vapor pressure and normal boiling point predictions for pure methyl esters and biodiesel fuels. Fuel 2005;84(7–8):943–50.
[40] Chung TH, Ajlan M, Lee LL, Starling KE. Generalized multiparameter correlation for nonpolar and polar fluid transport properties. Ind Eng Chem Res 1988;27(4):671–9.
[41] Chung TH, Lee LL, Starling KE. Applications of kinetic gas theories and multiparameter correlation for prediction of dilute gas viscosity and thermal conductivity. Ind Eng Chem Fund 1984;23(1):8–13.
[42] Ricart LM, Reltz RD, Dec JE. Comparisons of diesel spray liquid penetration and vapor fuel distributions with in-cylinder optical measurements. J Eng Gas Turbines Power 2000;122(4):588–95.
[43] Zandie M, Moghaddas A, Kazemi A, Ahmadi M, Feshkache HN, Ahmadi MH, et al. The impact of employing a magnetic field as well as Fe_3O_4 nanoparticles on the performance of phase change materials. Eng Appl Comput Fluid Mech 2022;16(1):196–214.
[44] Beale JC, Reitz RD. Modeling spray atomization with the Kelvin-Helmholtz/Rayleigh-Taylor hybrid model. Atomization Sprays 1999;9(6).
[45] Jafari B, Ashjaee N, Katoozian H, Tahani M. A comparative study of bone remodeling around hydroxyapatite-coated and novel radial functionally graded dental implants using finite element simulation. Medical Engineering & Physics; 2022, 103775.
[46] Liu Z, Yang L, Song E, Wang J, Zare A, Bodisco TA, Brown RJ. Development of a reduced multi-component combustion mechanism for a diesel/natural gas dual fuel engine by cross-reaction analysis. Fuel 2021;293:120388.
[47] Vishwanathan G, Reitz RD. Application of a semi-detailed soot modeling approach for conventional and low temperature diesel combustion–Part I: model performance. Fuel 2015;139:757–70.
[48] Vishwanathan G, Reitz RD. Development of a practical soot modeling approach and its application to low-temperature diesel combustion. Combust Sci Technol 2010;182(8):1050–82.
[49] Gad MS, Ismail MA. Effect of waste cooking oil biodiesel blending with gasoline and kerosene on diesel engine performance, emissions and combustion characteristics. Process Saf Environ Protect 2021;149:1–10. 0957-5820.
[50] Yusoff MNAM, Zulkifli NWM, Sukiman NL, Chyuan OH, Hassan MH, Hasnul MH, Zulkifli MSA, Abbas MM, Zakaria MZ. Sustainability of palm biodiesel in transportation: a review on biofuel standard, policy and international collaboration between Malaysia and Colombia. Bioenergy Res 2021;14(1):43–60.
[51] Yusoff MHM, Ayoub M, Jusoh N, Abdullah AZ. The challenges of a biodiesel implementation program in Malaysia. Processes 2020;8(10):1244.
[52] Johari A, Nyakuma BB, Nor SHM, Mat R, Hashim H, Ahmad A, Zakaria ZY, Abdullah TAT. The challenges and prospects of palm oil based biodiesel in Malaysia. Energy 2015;81:255–61.
[53] Ashnani MHM, Johari A, Hashim H, Hasani E. A source of renewable energy in Malaysia, why biodiesel? Renew Sustain Energy Rev 2014;35:244–57.
[54] Gad MS, El-Seesy AI, Radwan A, He Z. Enhancing the combustion and emission parameters of a diesel engine fueled by waste cooking oil biodiesel and gasoline additives. Fuel 2020;269:117466. 0016-2361.
[55] Feng Y, Xia Z, Huang L, Ma L. Effect of ambient temperature on the ignition and combustion process of single aluminium particles. Energy 2018;162:618–29.
[56] Kitano T, Nishio J, Kurose R, Komori S. Effects of ambient pressure, gas temperature and combustion reaction on droplet evaporation. Combust Flame 2014;161(2):551–64.
[57] Kafrawi F, Lee K, Zhang C, Bari S. Spray analysis of Palm-Based biodiesel to correlate performance and combustion analysis of a compression ignition engine. Fuel 2022;319:123822.
[58] Joshi MP, Thipse SS. Combustion analysis of a compression-ignition engine fuelled with an algae biofuel blend and diethyl ether as an additive by using an artificial neural network. Biofuels 2021;12(4):429–38.
[59] Sathiyamoorthi R, Sankaranarayanan G, Munuswamy DB, Devarajan Y. Experimental study of spray analysis for Palmarosa biodiesel-diesel blends in a constant volume chamber. Environ Prog Sustain Energy 2021;40(6):e13696.
[60] Li J, Yang W, An H, Zhao D. Effects of fuel ratio and injection timing on gasoline/biodiesel fueled RCCI engine: a modeling study. Appl Energy 2015;155:59–67.
[61] Liu H, Wang X, Zheng Z, Gu J, Wang H, Yao M. Experimental and simulation investigation of the combustion characteristics and emissions using n-butanol/biodiesel dual-fuel injection on a diesel engine. Energy 2014;74:741–52.
[62] Li J, Yang W, An H, Chou S. Modeling on blend gasoline/diesel fuel combustion in a direct injection diesel engine. Appl Energy 2015;160:777–83.
[63] Xu Z, Duan X, Liu Y, Deng B, Liu J. Spray combustion and soot formation characteristics of the acetone-butanol-ethanol/diesel blends under diesel engine-relevant conditions. Fuel 2020;280:118483.
[64] Kim K, Lim O. Investigation of the spray development process of gasoline-biodiesel blended fuel sprays in a constant volume chamber. Energies 2020;13(18):4819.
[65] Medina M, Fatouraie M, Wooldridge M. High-speed imaging studies of gasoline fuel sprays at fuel injection pressures from 300 to 1500 bar. 2018. SAE Technical Paper.
[66] Yu S, Yin B, Bi Q, Jia H, Chen C. Effects of gasoline and ethanol on inner flows and swallowtail-like spray behaviors of elliptical GDI injector. Fuel 2021;294:120543.
[67] Badawy T, Xu H, Li Y. Macroscopic spray characteristics of iso-octane, ethanol, gasoline and methanol from a multi-hole injector under flash boiling conditions. Fuel 2022;307:121820.
[68] Liu J, Feng L, Wang H, Zheng Z, Chen B, Zhang D, Yao M. Spray characteristics of gasoline/PODE and diesel/PODE blends in a constant volume chamber. Appl Therm Eng 2019;159:113850.

[69] Frenklach M, Wang H. Detailed modeling of soot particle nucleation and growth. In: Symposium (international) on combustion. Elsevier; 1991.
[70] Mahmoud NM, Yan F, Zhou M, Xu L, Wang Y. Coupled effects of carbon dioxide and water vapor addition on soot formation in ethylene diffusion flames. Energy Fuel 2019;33(6):5582–96.
[71] Choi B, Choi S, Chung SH. Soot formation characteristics of gasoline surrogate fuels in counterflow diffusion flames. Proc Combust Inst 2011;33(1):609–16.
[72] Park S, Wang Y, Chung SH, Sarathy SM. Compositional effects on PAH and soot formation in counterflow diffusion flames of gasoline surrogate fuels. Combust Flame 2017;178:46–60.
[73] Mahmoud NM, Yan F, Wang Y. Effects of fuel inlet boundary condition on aromatic species formation in coflow diffusion flames. J Energy Inst 2019;92(2):288–97.
[74] Mirhashemi FS, Sadrnia H. NO_x emissions of compression ignition engines fueled with various biodiesel blends: a review. J Energy Inst 2020;93(1):129–51.
[75] Putrasari Y, Lim O. A study on combustion and emission of GCI engines fueled with gasoline-biodiesel blends. Fuel 2017;189:141–54. 0016-2361.
[76] Ileri E, Atmanli A, Yilmaz N. Comparative analyses of n-butanol–rapeseed oil–diesel blend with biodiesel, diesel and biodiesel–diesel fuels in a turbocharged direct injection diesel engine. J Energy Inst 2016;89(4):586–93.
[77] Dwivedi G, Sharma M, Verma P, Kumar P. Engine performance using waste cooking biodiesel and its blends with kerosene and ethanol. Mater Today Proc 2018;5(11):22955–62.
[78] Dwivedi G, Jain S, Sharma M. Impact analysis of biodiesel on engine performance—a review. Renew Sustain Energy Rev 2011;15(9):4633–41.